

Special Section:

The Mars Perseverance Rover
Jezero Crater Floor Campaign

Key Points:

- In situ mapping from the rover observations on Mars uses field geologic mapping methods
- Documents the geologic context of samples and the crater floor traverse of Perseverance
- Develops methods applicable to future robotic and human traverses on planetary surfaces

Correspondence to:

L. S. Crumpler,
larry.crumpler@state.nm.us

Citation:

Crumpler, L. S., Horgan, B. H. N., Simon, J. I., Stack, K. M., Alwmark, S., Dromart, G., et al. (2023). In situ geologic context mapping transect on the floor of Jezero Crater from Mars 2020 Perseverance rover observations. *Journal of Geophysical Research: Planets*, 128, e2022JE007444. <https://doi.org/10.1029/2022JE007444>

Received 13 JUL 2022
Accepted 8 MAR 2023
Corrected 18 OCT 2023

This article was corrected on 18 OCT 2023. See the end of the full text for details.

Author Contributions:

Conceptualization: L. S. Crumpler, D. Shuster

Formal analysis: L. S. Crumpler, B. H. N. Horgan, J. I. Simon, R. C. Wiens, A. Udry, P. Russell, S.-E. Hamran, J. Bell III

In Situ Geologic Context Mapping Transect on the Floor of Jezero Crater From Mars 2020 Perseverance Rover Observations

L. S. Crumpler¹ , B. H. N. Horgan² , J. I. Simon³ , K. M. Stack⁴, S. Alwmark^{5,6} , G. Dromart⁷, R. C. Wiens² , A. Udry⁸ , A. J. Brown⁹ , P. Russell¹⁰, H. E. F. Amundson¹¹, S.-E. Hamran¹¹, J. Bell III¹² , D. Shuster¹³, F. J. Calef III⁴ , J. Núñez¹⁴ , B. A. Cohen¹⁵, D. Flannery¹⁶ , C. D. K. Herd¹⁷ , K. P. Hand⁴ , J. N. Maki¹⁴ , M. Schmidt¹⁸ , M. P. Golombek¹⁴, and N. R. Williams¹⁴ 

¹New Mexico Museum of Natural History & Science, Albuquerque, NM, USA, ²Department Earth, Atmospheric, and Planetary Sciences, Purdue University, West Lafayette, IN, USA, ³Center for Isotope Cosmochemistry and Geochronology, NASA Johnson Space Center, Houston, TX, USA, ⁴Jet Propulsion Laboratory, California Institute of Technology, Pasadena, CA, USA, ⁵Niels Bohr Institute, University of Copenhagen, Copenhagen, Denmark, ⁶Department of Geology, Lund University, Lund, Sweden, ⁷Laboratoire de géologie de Lyon: Terre, planètes et environnement, Université de Lyon, Villeurbanne, France, ⁸Department of Geosciences, University of Nevada Las Vegas, Las Vegas, NV, USA, ⁹Plancius Research, Severna Park, MD, USA, ¹⁰Department of Earth, Planetary, and Space Sciences, University of California, Los Angeles, Los Angeles, CA, USA, ¹¹University of Oslo, Oslo, Norway, ¹²School of Earth and Space Exploration, Arizona State University, Tempe, AZ, USA, ¹³Department of Earth and Planetary Science, University of California, Berkeley, Berkeley, CA, USA, ¹⁴Johns Hopkins University Applied Physics Laboratory, Laurel, MD, USA, ¹⁵NASA Goddard Space Flight Center, Greenbelt, MD, USA, ¹⁶Queensland University of Technology, Brisbane, QLD, Australia, ¹⁷Department of Earth and Atmospheric Sciences, University of Alberta, Edmonton, AB, Canada, ¹⁸Department of Earth Sciences, Brock University, St. Catharines, ON, Canada

Abstract In situ geologic context mapping based on rover and helicopter observations provides documentation of a nearly continuous record of geology and exposed surface structure over a 120 m-wide corridor along the traverse of the *Mars 2020/Perseverance* rover. The results record the geologic context of Mars 2020 campaign sites and sample sites, including the local extent of bedrock outcrops, stratigraphy, attitude, and structure from imaging and rover-based remote sensing, and outcrop lithology based on in situ proximity science. Mapping identifies a sequence of igneous lithologies including (a) early mafic, possibly intrusive, rocks; (b) pervasively fractured and deeply altered massive bedrock of undetermined protolith; (c) buried and exhumed lava flows with pahoehoe and aa textures; (d) several varieties of regolith; and (e) small impact craters.

Plain Language Summary Reconnaissance-type geologic mapping along the traverse of Perseverance on the Jezero Crater floor is adapted from field geologic methods used on Earth and modified to account for the geometry of rover-based imaging. The final field geologic map records bedrock and surficial geology, contacts, and structures over a 120-m wide strip along the traverse. Most of the lithologies are igneous, including possible intrusive mafic rocks, deeply weathered massive rocks of unknown original lithology, and lava flows. Stratigraphy determined from mapping together with the observed inclination of layers identifies either uplift or draping of the section centered in the elevated older terrain. The final map information provides ground-truth geologic context for the first eight samples collected for return to Earth.

1. Introduction and Background

Increases in traverse lengths and data collected by current rover challenge the ability to organize, retrieve, and efficiently digest the context of each observation, surface measurement, and a sample collected in a format convenient for later analysis. This challenge will increase with future robotic and human exploration missions. In situ geologic context mapping (GXM) described here addresses this problem using both the heritage of recording geologic relationships on Earth in standard geologic field and reconnaissance mapping methods, and previous experience in rover-based in situ mapping performed throughout the *Mars Exploration Rover* mission (Crumpler et al., 2011, 2015).

© 2023. The Authors.

This is an open access article under the terms of the [Creative Commons Attribution-NonCommercial-NoDerivs License](https://creativecommons.org/licenses/by/4.0/), which permits use and distribution in any medium, provided the original work is properly cited, the use is non-commercial and no modifications or adaptations are made.

Investigation: L. S. Crumpler, B. H. N. Horgan, J. I. Simon, K. M. Stack, S. Alwmark, G. Dromart, R. C. Wiens, A. Udry, A. J. Brown, H. E. F. Amundson, D. Shuster, J. Núñez, B. A. Cohen, D. Flannery, C. D. K. Herd, M. Schmidt
Methodology: L. S. Crumpler
Resources: R. C. Wiens, J. Bell III, F. J. Calef III, K. P. Hand, J. N. Maki, M. P. Golombek, N. R. Williams
Validation: D. Shuster
Writing – original draft: L. S. Crumpler
Writing – review & editing: L. S. Crumpler, J. I. Simon

During the first 370 sols of operation on the surface, *Perseverance* pursued a science campaign along a 4.5 km traverse on the floor of Jezero Crater to document the geologic history of the crater floor as it relates to the delta (Farley et al., 2022; Sun et al., 2022; Wiens et al., 2022). Throughout the traverse a nearly continuous record of the local geologic context was acquired with in situ lithostratigraphic GXM, more commonly known as geologic “field mapping,” based on observations from *Perseverance* and interpretations of the lithology from available in situ observations and local measurements. GXM results provide a means of correlating observations from site to site and integrating the results of local investigations in context with wider observations. GXM also serves an important goal of the Mars 2020 mission to document the geologic context of returned samples and sites by characterizing the processes that formed and modified the geologic record within a field exploration area on Mars selected for evidence of an astrobiologically relevant ancient environment and geologic diversity and to obtain samples for which the field context is documented.

Comprehensive documentation of the geological setting from in situ observations is also a recognized need for documentation of returned samples by “*preemptively acquiring as much contextual information as possible of potential targets bearing biosignatures while “in the field” and “acquired through careful in situ field observations at multiple scales across the area in which the signatures occur”* (MEPAG E2E-iSAG, 2011). Local field context is a critical component—in conjunction with planetary-scale context and returned sample science—to develop our scientific understanding of Mars (Beatty et al., 2019).

This argument also holds true for any instrument observation of a surface in which later analysis may benefit from knowledge of the local geologic setting and the ability to compare the context of similar results at different locations. A salient attribute of GXM is its “preemptive acquisition of context data” in a compact record of the data in an easily digested graphical record of relationships in the field that may only be recognized as critical to analysis in later phases of the mission or as analysis of results unfolds in the future.

2. In Situ (GXM) Mapping Methods

A continuous lithostratigraphic geologic strip map or geologic transect was generated from rover observations during the Crater Floor Campaign (Sun et al., 2022) traverse from the *Octavia E. Butler (OEB) Landing Site* southward to the oldest identified terrain, “Séítah,” using Navcam orthographic mosaics (“orthomosaics”) as the near-field map base and Mars Reconnaissance Orbiter High-resolution Imaging Science Experiment (MRO/HiRISE) data as the far-field map base. In situ geologic mapping (GXM) is rooted in field geologic transect mapping methods used for at least 200 years on Earth during reconnaissance geologic mapping in previously unmapped terrains. Reconnaissance transects differ from quadrangle mapping because lateral contacts and lithologies in the outcrop are not followed and observations may only occur during a linear traverse with local walk-about (J. W. Barnes, 1991; Compton, 1985). Within a specific distance, lithologies may be visibly compared with confidence in proximal science lithologic identification done on exposures in the near field along the traverse. This confidence degrades with distance in accordance with the decrease in object resolution and incidence angle of view. Despite this limitation, a record of the observations as a geologic map is useful for recording the location and specific geologic context of observations, for the correlation of observations from site to site, and for expansion of local stratigraphic assessments and descriptive comparisons to a graphical representation of the results of continuous observations along the traverse. In situ geologic mapping force examination, hypothesis testing, and contextualization of all elements of the rover surroundings, often capturing significant relationships and outcrop details that are overlooked from a cursory analysis of individual images or instrument observations.

2.1. Rover-Based Mapping

In situ (field) geologic mapping is distinct from the *photogeologic mapping* that has been a principal method for identifying geologic relationships on the surfaces of planets since the early years of spacecraft exploration. *Photogeologic* maps are inferences about geology based on the morphology of the terrain exposures at scales observable from high altitude or orbit. *In situ geologic maps* are data records of lithology determined from direct physical contact with outcrops on the ground and, similar to field geologic mapping on Earth. In situ geologic mapping relies on the examination of geologic materials in outcrops on the surface for identification. It relies on traverses to identify contacts between differing mappable geologic materials. Mapping is done using the USGS definition of mappable units: “a geologic unit is a three-dimensional body of earth material, recognized by its

lithologic content (consolidated rock or unconsolidated sediment) and its boundaries at the surface and (or) subsurface” (U. S. Geological Survey, 1958).

As with field geologic mapping on Earth, in situ rover-based mapping matches the macroscopically identified (hand specimen) material from an outcrop or proximal workspace with what is visible from the rover remotely imaged in the local terrain. This is followed by recording on a base map the relevant geometries and locations of structures, exposures, and contacts between distinct lithologies. The compilation of in situ geologic maps here makes use of all instrument observations on Perseverance. The panoramic cameras (Mastcam-Z) (Alwmark et al., 2023; Bell et al., 2022; Bell & Maki, 2021) and Navigation cameras or Navcams (Maki, 2020; Maki et al., 2021) provide the base to recording mappable geologic units, while contact science instruments, SHER-LOC (Bhartia et al., 2021; Beegle, 2021), PIXL (Allwood et al., 2020) and rover-based remote sensing instruments (SuperCam LIBS and RMI) (Maurice et al., 2021; Maurice & Wiens, 2021; Wiens et al., 2020), provide confirmation of lithologic details in the far field.

Supercam RMI data plays an important role in providing continuity of lithologic detection along the traverse analogous to periodic megascopic checks of lithology that are performed during a traverse on Earth. On Earth, it is common practice to examine unprepared samples along a traverse simply to fill in the gaps between actual stops with detailed outcrop examination. Likewise, because not every outcrop is examined in detail during mapping with proximity science and contact instruments, the confirmation of lithologies along the traverse between stops is important.

2.1.1. Identifying and Recording Levels of Mapping Confidence

Because observations acquired of geologic context close to the rover are more accurate in both location and in assessment of the lithology than those farther away, the distance outward from the rover that mapping of a given confidence level is warranted is determined by the resolution and viewing incidence from the point of observation (rover). These properties vary across the image, unlike the mostly uniform resolution and consistent incidence angle of an orbital image used in photogeologic mapping. The relative levels of accuracy of the near-field versus far-field mapping are assigned by indexing five levels of mapping accuracy and reliability on the final map. The specification of levels identifies the influence of the variation in data quality and mapping fidelity from the rover perspective based on resolution and viewing geometry.

From previous experience in rover-based in situ mapping, a terrain resolution of 1–2 cm pixels (Crumpler et al., 2015, 2020) and an incidence of approximately 4° or greater are required to confidently identify distal outcrops of a lithology previously characterized in the proximal outcrop. In practice, it has been found that terrain relief and surface roughness may have a larger impact on the distal lithologic identification and mapping than resolution alone. Simply increasing resolution does not resolve the distant geologic characteristics significantly better than lower resolutions at the same or similar distance. Local relief and surface roughness on the order of 10 cm can result in occlusions over much of the surface at lower incidence. The influence of these parameters remains to be assessed and is ongoing.

During a typical drive, the navigational camera (Navcam) is the panoramic camera most frequently used on Mars 2020, and for which there is the greatest azimuthal coverage at every stop along the rover traverse. The highest resolution of the Mars 2020 color Navcam is 0.33 mrad, yielding an approximate resolution of 1 cm at 30 m where the incidence is less than 4° (Figure 1). This established a nominal mapping range for GXM of 30 m, resulting in a mapping swath 60 m wide along the traverse path at this confidence level. Other higher resolution Mars 2020 cameras and instruments (e.g., *Mastcam-Z*, *SuperCam VISIR*, and *RMI*) provide proximal macroscopic lithologic identification and additional detection and confirmation of far field lithofacies, but Engineering Camera (EECAM) data, particularly the Navigation Cameras (Navcams), are the commonality between stops making it the most common comparative data set for correlating geology from one site to another.

In addition to Navcams, both the front and rear Hazard Avoidance Cameras or Hazcams are also applicable for recording the near field and are useful for identifying outcrop-scale geologic details in the workspace at sites where proximity science activities and sampling occur. Hazcam resolutions can exceed Navcam resolution within the typical workspace (Maki et al., 2021).

Details of the expected geometry, resolution, and utility of each level in operations for specific sol templates are summarized in Figure 1. Levels 5 and 4 are precision maps, have the highest confidence of being archival quality

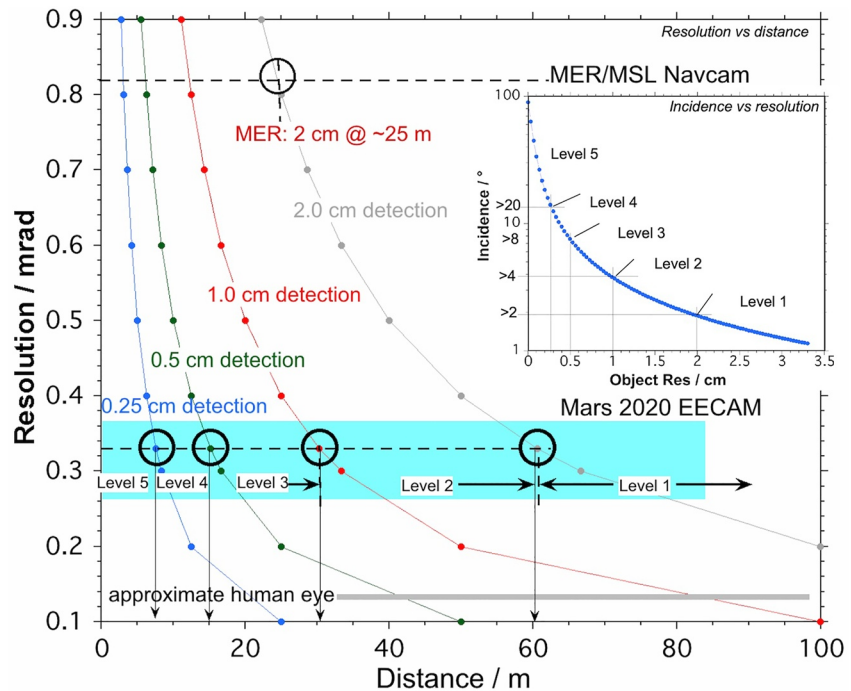


Figure 1. Camera resolution as a function of distance, identifying the characteristics for MER-MSL Navcams and for Mars 2020 EECAMs. Inset: In situ mapping confidence levels 5 through 1 defined according to the resolution and angle of optical incidence.

records of observables, and are applicable to correlating the observations from proximal science targets with characteristics of associated variations in the local bedrock. Mapping becomes progressively more comparable to outcrop mapping at higher levels, 4 through 5. This becomes comparable to standard field geologic mapping and reconnaissance mapping at lower levels 3 through 2.

2.1.2. Characteristics of Mapping Confidence Levels

The following section discusses the differences in the information recorded in each level and the characteristics of mapping in the five mapping levels identified. The geometric characteristics are summarized in Table 1 and illustrated in Figure 1.

Level 5 is the highest level of map accuracy and is equivalent to outcrop mapping on Earth. The rover chassis blocks 20–30° azimuth.

Description: Extremely high-resolution outcrop-scale geologic mapping based on near-field images.

Instruments used: EECAM Hazcams, Navcams, and Mastcam-Z macroscopic and microscopic outcrop observations via SHERLOC/WATSON/PIXL/SuperCam VISIR and RMI; includes data from SuperCam LIBS and Raman capabilities; includes contact science results and target locations.

Characteristics mapped: Millimeter-scale outcrop contacts and structures; lenses and sedimentary microstructures; larger float rocks; mappable differences in regolith; attitudes of planar structures, especially using down-dip methods; vesicle distributions and sizes; lava surface textures; and fracture patterns. This level of mapping also includes smaller regions of interest within an outcrop, for example, a map of SHERLOC data or a petrographic map.

Table 1
Characteristics of Mapping Confidence Levels

Mapping level	Radius/m	Pixel size/cm	Incidence angle+ ^a
5	<7.5	<0.25	87–20 ^b
4	<15	<0.5	>8
3	<30	<1	>4
2	<60	<2	>2
1	<120	>2	2~1
0	na	~24	~vertical

Note. + measured from horizontal.

^a~25° azimuth near-field at rover frame azimuth ~180–200 occluded by rover chassis. ^bSurface mapping limited by chassis to ~87° maximum from mast cameras.

Earth field equivalent: Similar to large-scale outcrop mapping, outcrop sketches, mapping contacts and structures at one's feet and recording sample locations in the immediate surroundings out to ~7.5 m.

Level 4 is high resolution geologic mapping, contacts are high precision similar to Level 5 but are based on in situ remote sensing only; local terrain may occlude outcrop detail. Similar to the limits of field geologic mapping to one's immediate left and right during a traverse on Earth. The rover deck blocks 20–30° rover-frame azimuth.

Description: The incidence angle is significantly greater than Level 5 but contacts may still be discerned at millimeter scale. The macroscopic outcrop and near-field geologic mapping within Level 4 space may be suitable for proximity and contact science target selection.

Instruments used: EECAM and Mastcam-Z, SuperCam VISIR and RMI.

Characteristics mapped: Resolution is sufficient to extend the identified lithologic mapping and contact science from Level 5 space, but the inferences are not directly testable with the in situ instruments, including millimeter-scale outcrop contacts and structures, lenses and sedimentary microstructures, larger float rocks, mappable differences in regolith, and bedding and structure plane attitudes are measured.

Earth field equivalent: Similar to informed interpretation of terrain immediately adjacent to a geotraverse, the trace of contacts confirmed at the outcrop is detectable in the adjacent terrain out to ~15 m.

Level 3 is a high confidence record of the lithology within the rover local field of observation based on existing knowledge of the recurring lithologies and their physical attributes as seen in cameras.

Description: Level 3 is a lower confidence map that extends the results from Levels 5 and 4 into the surrounding terrain but does so based on a fraction of the data available for Levels 5 through 4; some discriminants are missing, but there is significant confidence that the remaining attributes are sufficient for identification of the given lithology; contacts are located with centimeter accuracy.

Instruments used: EECAM and Mastcam-Z, SuperCam VISIR and RMI.

Characteristics mapped: Contacts between distinctive lithologies, regolith cover, obvious structures; extensions of Level 5-4 contacts.

Earth field equivalent: Similar to identifying the lithology of an outcrop across a creek or on the other side of a canyon out to ~30 m; there is high and arguable confidence in the identification based on physical character of exposures compared with distal characteristics, but the interpretation is not directly confirmed.

Level 2 mapping takes place in important regions of interest and takes advantage of sites of extended outcrop campaigns to make educated guesses about the contacts in the far-field. This information gives a more expansive context to data acquired at an important location.

Description: Contacts are located with centimeter to ten-cm accuracy; new lithologies not examined before may be undetected, but familiar lithologies are mapped.

Instruments used: EECAM and Mastcam-Z, SuperCam VISIR and RMI.

Characteristics mapped: Contacts and structures identified within Levels 5 through 3 that are regional and easily identified at distance.

Earth field equivalent: Reconnaissance geologic mapping based on local identifications of lithologies and structures from a drive- or rapid hike-through type traverse. Geologic characteristics are identified from afar using physical outcrop characteristics associated with a given lithology.

Level 1 is reasonable geologic inference where there is no data, as between outcrop exposures and is analogous to dashed line contacts in field geologic maps.

Description: This mapping fills in the traverse between waypoints and stations with low fidelity mapping based on an extension of in situ results. It is Level 1 mapping that will result in a continuous strip map along the path of the rover from the first to the last sol of traverse.

Instruments used: Mastcam-Z, SuperCam VISIR and RMI.

Characteristics mapped: Major lithologies, contacts, and stratigraphic relationships.

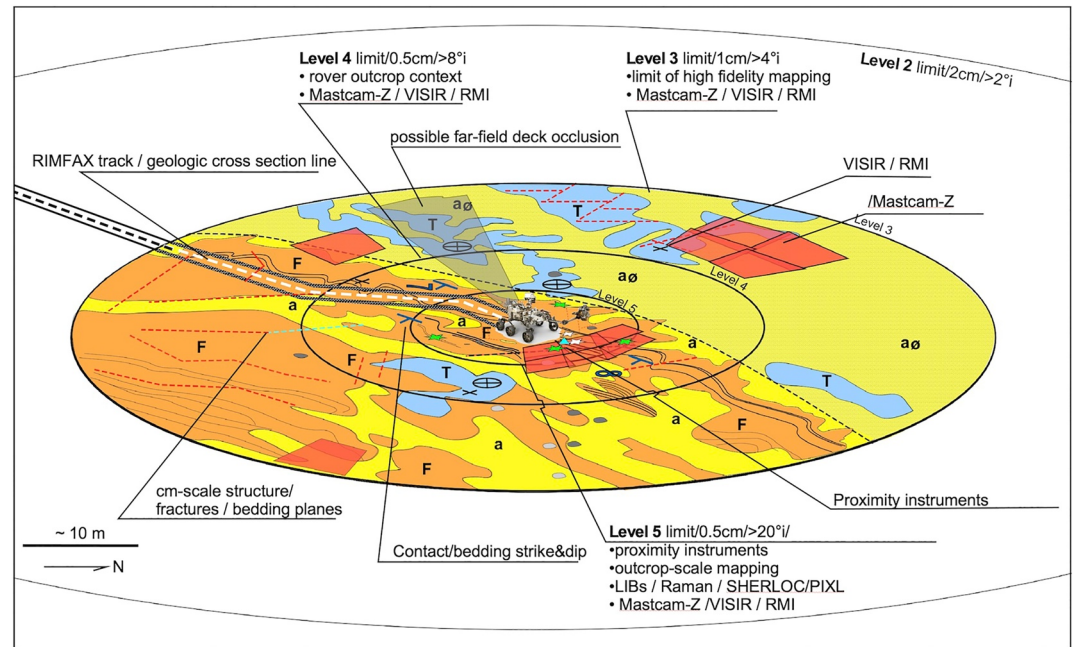


Figure 2. The model of the geologic context mapping concept showing an in situ lithologic map and unit attitudes from rover-based observations at one station. Nested levels of outward-decreasing mapping confidence and resolution are illustrated together with the types of instrument observations that may be applicable at each mapping level.

Earth field equivalent: Geological inferences in areas of cover between areas of exposed bedrock.

Level 0 is photogeologic mapping in which features are observable from the rover but no GXM inferences are possible at resolutions equal to or better than orbital observations by MRO/HiRISE. This method captures units defined by differences in terrain physical characteristics and carries no identified lithologic information unless supplemented with mineral and chemical data derived from orbital remote sensing, such as MRO/CRISM.

The application of these five levels of mapping is illustrated with a hypothetical example of one station (Figure 2). The mapping captures differing levels of in situ geologic mapping information and a data set of known reliability while providing context for instrument science and tactical insights. The nested levels of mapping are based on a combination of imaging camera results (Level 3 through 1), elemental and mineralogy remote-sensing instruments (up to Level 4), and high-resolution map scale contact and proximity instrument results (up to Level 5). Reliable mapping occurs within Level 3, and Levels 4 and 5 are refinements. Level 2 mapping is useful for far-field context but relatively poorly constrained relative to the higher levels yet may still identify the important lithologies and contacts. Level 1 mapping is essentially “dashed line” contact mapping of the regions and relies heavily on orbital images to both contact location and unit correlation relative to observations closer to the rover. It can be useful for projecting important relationships into the surrounding region but carries with a corresponding decrease in reliability as an accurate record.

2.1.3. Example of In Situ Mapping Applied

The application of these methods in recording in situ geologic data as geologic maps is illustrated in Figure 3. The steps used to transfer information from the outcrop and panoramas to the map are (a) acquire panoramic Navcam mosaic of surroundings, preferably with terrain modeling available or accurate ranging positions of geologic information to be recorded; (b) the position of the rover is identified on a base map; (c) use textural characteristics of outcrops and rocks together with the proximal science instruments and team discussion to interpret the lithology from the mineral, chemical, and physical characteristics of exposed bedrock. This includes use of data from Mastcam-Z, SuperCam, PIXL, SHERLOC, WATSON to determine the macroscopic and microscopic character of a mapped unit; (d) identify the visible characteristics of the outcrop in the panoramic image data for which a lithology has been determined; (e) correlate these physical characteristics and visible hand specimen petrology with all possible exposures in the panorama as perspective-based maps much like outcrop sketching (Figure 3a);

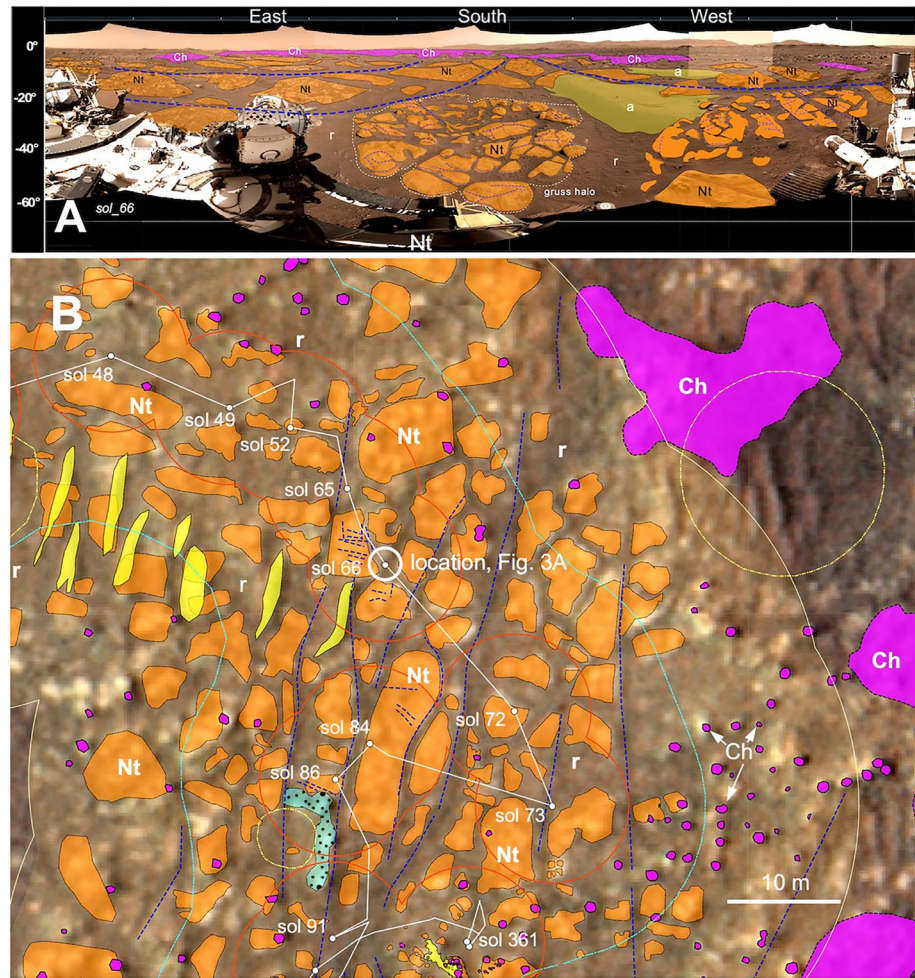


Figure 3. (a) Navcam mapping perspective. Perspective-based geologic mapping of a single Navcam 360 panorama from the sol 66 (site 3 drive 2208) location, here south-centered, showing the distribution of polygonally jointed bedrock outcrops (Nt), intervening grus haloes and regolith (r), aeolian bedforms (a), and an overlying dense and fractured basaltic sheet (Ch) in the distance. Camera elevation angle and azimuth with respect to the north on vertical axis and horizontal axis, respectively. Units shown are discussed in Sections 3.1.1 and 3.2.1. N_LRGB_0066_RAS_0032208_CYL_S_COLORRPJ01. (b) geologic context mapping results in A reprojected onto the local Navcam orthomosaic image, merged with Navcam orthomosaic image and mapping from previous and subsequent sol positions, and recorded as geologic mapping on the regional MRO/HiRISE base image. The map is centered on the sol 66 location. Legend as in Figure 5.

(f) establish the location of the division line (contact) between physical lithologies within the field of the panoramic camera, for example, the contact between an outcrop consisting of a lithologic unit established from in situ contact or in situ local remote sensing science and the surrounding regolith, or the contact between a known lithology and an adjoining bedrock material of differing physical or spectral character. The location of contacts and structures identified is transferred to the orthographic map base (Figure 3b) using stereo image range mapping; and (g) these data are recorded in GIS on the relevant base, the MRO/HiRISE image and Digital Terrain Model georeferenced to the M2020 Team defined “Jezero Crater Projection map.” The projection is a version of the special Mars 2020 MRO/HiRISE base mosaic, discussed by Ferguson et al. (2020), using an orthographic map projection centered on the landing site (77.4298 Lon, 18.4663 Lat).

Because Navcam orthomosaics are acquired throughout the traverse, the resulting base of Navcam orthomosaics is then used to supplement the regional MRO/HiRISE image base with centimeter-scale resolution within 60 m of Perseverance end-of-drive locations (Figure 4a). The compilation of individual GXM maps for each Navcam mosaic then provides a complete high-resolution map of the geologic units or transect over the length of the traverse (Figure 4b).

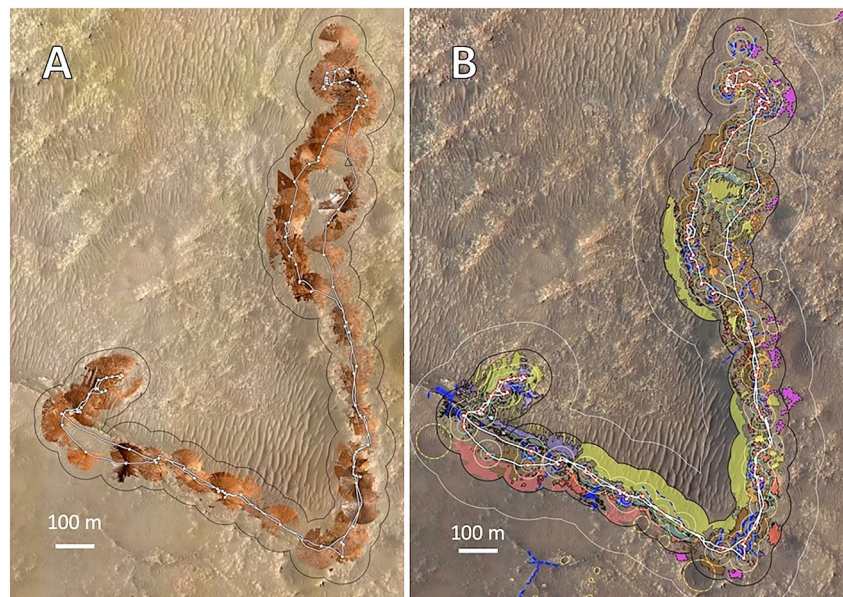


Figure 4. (a) Distribution of Navcam orthographic mosaics (45 m radius) acquired along the traverse (Sols 001–370) georeferenced to the regional Mars 2020 Jezero Crater floor MRO/HiRISE mosaic. Black line boundaries are the 60 m-radius (Level 2) mapping limits. (b) geologic context mapping mapping compiled along the traverse length at each location for which a Navcam orthomosaic was acquired. The result is a geologic strip map, or a reconnaissance field geologic map, determined from the perspective of *Perseverance* showing lithologies and stratigraphic relations in the surrounding terrain within 45–60 m of the traverse. White dots are post-drive sol locations. White line boundary is the 120 m-radius (Level 1) mapping limit. Concentric circles around each sol location indicate Levels 1–5. See Figure 5 for map key.

3. GXM Results From Sol 001 to 370

3.1. Summary Field Descriptions and Stratigraphy of Lithologies Mapped

The following briefly reviews the distinct lithologies identified during the crater floor traverse identified from in situ inspection of outcrops and isolated samples. These were categorized by correlating exposures from site to site along the traverse, followed by the development of stratigraphic models by the science team (Farley et al., 2022; Wiens et al., 2022) and their occurrences (Table 2). The purpose here is to provide a reference to the field description of the physical characteristics and textures (“lithomorphology”) used for detecting distinct lithologies.

Mapping prior to landing (Stack et al., 2020; Sun & Stack, 2020) established two regional crater floor units in the vicinity of the landing site. In Sun & Stack, 2020, the lowest crater floor unit in the area of the landing site, “lower etched unit, Nle,” correlates with the terrain identified as “Séítah” in the mapping in this work *and was described as* containing northeast-southwest-oriented ridges that extend several hundred meters in length and characterized in orbital spectral remote sensing by association with identified olivine and carbonate, and craters generally greater than 200 m in diameter. They identified Nif as the “Jezero crater floor unit” which overlies and embays the lower etched unit Nle. Njf correlates with the unit identified as “Máaz” in this work.

Stack et al. (2020) describe more detailed photogeologic mapping (see their Figure 5) by the *Perseverance* science team prior to landing for scientific hypothesis development and strategic planning for *Perseverance*’s exploration of Jezero crater. The same units described above were defined as “crater floor fractured, rough” (Cf-fr) and an older unit as “crater floor fractured” (Cf-f/1). “Crater floor fractured, rough” (Cf-fr), equivalent to Nif of Sun & Stack, 2020, also correlates with the unit “Máaz” in this work and is described as being a light-to medium-toned, rough, boulder-producing unit that is highly crater-retaining in which polygonal fracture networks are common. It also overlies “Crater floor fractured (Cf-f/1),” equivalent to “lower etched unit,” Nle of Sun & Stack, 2020. Crater floor fractured (Cf-f/1) was described as consisting of massive, light-toned fractured and blocky bedrock exposed on the crater floor below $-2,530$ m elevation.

Both units defined in the previous mapping above were directly observed in the rover observations resulting in greater precision of the contact locations established in prior photogeologic mapping and in situ determination

Table 2

Narrative Summary by Sol Position of Principal Terrain and Map Units Traversed, Observation Targets, Abrasion Sites, and Samples Collected

Mission sol	Traverse distance	Activity/principal observations	Targets, Abrasions & Samples
1–14	6.25 (unit Nt)	Landing site observations, Regolith bearing vesicular cobbles, granular textured polygonal-jointed outcrops, some bearing a concentric exfoliated appearance	Máaz, Tselhchee, vesicular cobbles and fine regolith
14–20	87.24 (unit Nt)	Traverse to heli shield drop, regolith and exfoliated polygonal outcrops; dark upper relief on outcrops increase eastward	Yeehgo, Iina
23–29	9.41 (unit Nt)	Short drive to positions nearby on granular textured polygonal-jointed; many polygonal-jointed outcrops grade upward to darker, less granular upper surfaces or dark protuberances	
31–44	88.14 (unit Nt)	Return to landing site to deploy and image heli; local polygonal rocks and intervening regolith bearing small vesicular cobbles	Hedgehog, Beavertail,
47–52	79.25 (unit Nt)	Drive east to heli observation site at Van Zyl Overlook, continue observations on granular textured polygonal-jointed outcrops, also referred to as “pavers,” many of which have a concentric exfoliation structure	
65–73	29.3 (unit Nt)	Drive southeast through field of granular, exfoliated polygonal outcrops and large fractures, distal observations of high-standing dark outcrops, RIMFAX sounding across fractures	Nataani
84–86	23.14 (unit Nt)	Unusual float rocks clustered around degraded small impact crater	Hoolhnili, Hastah_tsaadah, Tsostid_tsaadah
91–100	19.67 (unit Nt)	Traverse south-southwest parallel to strike of fractures	
102–105	137.16 (unit rp)	Traverse along low, regolith covered terrain toward Adziilii Crater; regolith contains unusual abundance of pebble-size clasts; slight rise to west consists of large float blocks isolated with regolith	Mixed and coarse varieties of regolith
107–116	221.46 (units rr, r, Nt)	Traverse south along west side of Adziilii Crater in extensive regolith materials inboard of escarpment abutting Séítah; RIMFAX sub-surface sounding identifies dense layer dipping 10° eastward; large block (Taa tsaadah) in ejecta exhibits likely ropey texture suggesting dense layer is basalt excavating by Adziilii Crater	Contact between mixed regolith and fine regolith; Whila, first target on Rochette type basalt; Taa tsaadah, ropy basalt ejecta block
122	30.4 (unit rp)	First test of “autonav” driving; avoided up-ended tabular basalt with vesicle abundance gradient; well-exposed blocks bearing vesicle sheets in escarpment to west;	
122–124	80.99 (unit rr, Nt, Ro)	Traverse along contact zone between granular polygonal lithology and basalt; vesicular basalt surface dipping gently to the east	Naltsos
124–129	119.35 (unit r, Ro)	Traverse along contact zone between granular paver lithology and escarpment basalt	Kad, Raton
130–131	231.3 (unit rr)	Traverse in “autonav” along contact zone between granular polygonal lithology and rocky regolith with mixed vesicular basalt float and outcrop west of traverse path	
131–134, (353mid-354mid)	200.56 (unit r)	Presence of granular polygonal lithology abruptly discontinues; vesicular escarpment basalt is proximal to high-standing dark basalt; local vesicular float rock (Castellane) displays gradient in vesicle size distribution consistent with an upper basalt section	Castellane
134–153	277.74 (unit r, Ru)	Traverse drops eastward down to granular polygonal lithology with high-standing dark rocks capping slope to the east; intervening vesicular dark high-relief tops on polygons proximal to slope; first coring test activity	Champs, Beaujeu

Table 2
Continued

Mission sol	Traverse distance	Activity/principal observations	Targets, Abrasions & Samples
155–157	51.05 (unit Ru)	Traverse to polygonal outcrops north of Mure for first attempt at sample coring activity; Bump to a selected granular outcrop polygon and proximal science activities; abrasion followed by Watson/Sherloc/PIXL observations and subsequent coring attempt	<i>Abrasion: GuillaumesSample: Roubion (atmosphere)</i>
168	31.87 (unit r, Ro)	Traverse south to the contact between the granular polygon materials and an overlying horizontal foliations and vesicle sheets in basalt over granular polygon terrain at Mure	Baume
169–170	157.81 (unit r, Ru, Ar?, a)	Commence traverse westward along base of Artuby Ridge; drive moved down a small escarpment on the edge of the granular polygon terrain during sol 170 drive onto a dusty regolith-covered slope between Artuby Ridge and Séítah/dunes; remote observations of escarpment south of rover	Lattes
171 (351mid)	111.87 (unit S)	Continue traverse along dusty regolith-covered slope between Artuby Ridge and Séítah/dunes; local exposure examined by Supercam	Entrevaux
173–175	59.89 (unit r, Ar)	Drove to proximity with escarpment exposure of horizontally laminated granular rocks in north face of Artuby Ridge; RIMFAX detects reflectors dipping southeast approaching Artuby escarpment; local slump fault cuts outcrop	Grasse
177–178	175.76 (unit r, Ar, Ro)	Approach drive southwest onto Artuby Ridge; dark horizontally laminated outcrops observed along crest of ridge at approach point	Sauze
180	10.97 (unit r, Ro)	Drove onto Artuby Ridge at Castille, abrasion on Bellegarde followed first successful sample coring at Rochette; 2 samples, Montdenier, Montagnac	Estoublon, Digne, Lance, Souche, Pont, <i>Abrasion: BellegardeSamples: Montdenier, Montagnac</i>
199–200	242.49	Long traverse northwest to point on Artuby Ridge for descent to Séítah	Digne
201–202	87.44	Descend north from Artuby Ridge and began traverse northeast into Séítah terrain	Rourebél
203–204	46.36	Traverse to laminated outcrop exposure, Bastide, near base of hill within Séítah terrain	Bastide, Garde, Levens, Monier, Cine
210	52.35	Began traverse around west flank of hill to Marte-Caille region near top of hill; stopped at this location for solar conjunction stand down	
237–238	50.39	Traversed eastward to base of Vignols hill/ridge exposing finely laminated dark rocks capping upper slopes of hill within Séítah terrain	Villeneuve, Cheiron, Content
239–248	12.36	Drove to prominent laminated outcrops capping Caille hill; abrasion on Brac (Dorbes) followed by Sherloc and PIXL; second sample coring activity samples Salette, Coulettes. Observations on Caille exposures to northeast	Brac, Valette, Ubraye <i>Abrasion: Dorbes,Samples: Salette, Coulettes</i>
278	6.34	Bump forward onto ridge top for observations on vesicular basalt target Hotel	Hotel, Rent, Thouron
280	36.26	Return drive west from Brac area, remote observation on outcrops near margin of prominent east-west fracture; laminations dip southeast $\sim 10^\circ$	Villar
281–283	40.24	Departure drive from Séítah ridge, remote observations on local rocks near base of a Séítah hill	Norante, Rougon
285–328	74.73	Approach southwestward-dipping outcrop Issole at base of Aruby Ridge near contact between Séítah and Artuby Ridge; third sampling site, abrasion Quartier followed by samples Robine and Malay on sols 333-335	Castiglone <i>Abrasion: Quartier,</i>

Table 2
Continued

Mission sol	Traverse distance	Activity/principal observations	Targets, Abrasions & Samples
333–335	22.52	Bump to south side of Issole outcrop for access to upper layers with samples Robine, Malay	<i>Samples: Robine, Malay</i>
340	237.78	Rapid traverse up onto Artuby Ridge and back toward Citadelle with mid-drive imaging along the way	
341–343	292.75	Rapid drive off Artuby Ridge onto slope along Séítah south margin through Citadell and southeasterly to exposure of Artuby laminated outcrops at Rimplas for proximal science observations on the outcrop	Rimplas
351	92.4	Rapid drive with mid-drive imaging past Roubion/Mure area onto granular polygonal outcrops along southeastern margin of Séítah (“paver valley” area)	
352–353	526.25	Rapid drive north and up onto eastern margin escarpment with stop for inspection of potential dark, high-standing basalt exposure	
354–355	454.44	Continued rapid drive traverse north between high-standing dark rocks on the east, granular polygons along the drive, and escarpment vesicular blocks on the east; traverse forked to the east side of Adziilii Crater	
359–360	250.48	Rapid drive stops on east edge of Adziilii Crater ejecta and northeast side, continuing northward along granular polygons to vicinity of fourth sampling location a few meters east of the sol 91 location.	
361–362	28.85	Drive and approach to abrasion target Alfalfa and samples Hahonih and Atsah on fourth sample target Sid, an example of an outlier dark, high-standing rock resting on a terrain of granular polygons	<i>SidAbrasion: AlfalfaSamples: Hahonih, Atsah</i>
379	198.83	Rapid drive continued north through regolith-dominated terrains toward the delta front by way of skirting around eastern margin of Séítah	

Note. Unit abbreviations (Nt, rr, etc.) are defined in Figure 5 geologic map explanation of units.

of their actual distinct lithologies, Perseverance landed in the Jezero Crater floor (Nif) (or crater floor fractured rough, Cf-fr) photogeologic unit 150 m east of its contact with the lower etched unit Nle (or crater floor fractured unit, Cf-f/1). After initial in situ examination of the lithologic diversity and prominent exposures with continuity over the traverse, informal stratigraphic unit names were assigned to the younger and older photogeologic units, *Máaz* formation (Cf-fr) and *Séítah* formation (Cf-f-1) respectively. These formations were further divided into members based on morphological and textural differences (lithomorphologies) in outcrops, each generally further characterized as distinct lithologies during the course of subsequent proximity science observations (in situ measurements).

Materials identified and mapped include several varieties of surficial and regolith deposits and 8–9 bedrock lithologies. Names given to distinct geologic lithomorphologies encountered and shown on the maps here are based on the mission target names of outcrops or individual rocks where the specific lithology was first analyzed sufficiently to warrant distinction from other materials observed. The informal formation and member names assigned and used throughout this discussion follow general stratigraphic naming conventions from mapping on Earth (e.g., AIPG, 1961; Cohee, 1974).

3.1.1. Surficial Units

Three varieties of “unconsolidated sediments or regoliths” are recognized (Table 3) (Vaughan et al., 2023), *fine*, *coarse*, and *mixed*, based on grain size measurements from Mastcam-Z and Watson. An attempt was made to map examples of these that were greater than a few meters in extent and largely with Levels 5 and 4. Smaller areas occur throughout the traverse that are not depicted in the in situ mapping.

Table 3
Field Description of Regolith Units Mapped

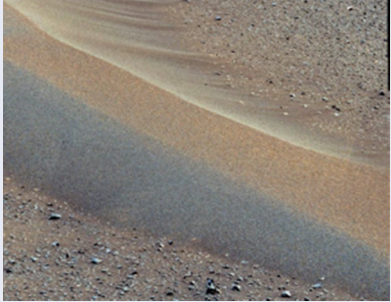
In situ map name/unit	Description	Field interpretation	Example from traverse
Aeolian Bedforms	Ripples, dunes, drifts of fine-grained & sand-sized (~0.08 mm–0.53 mm) regolith and mixed dust	Sand moved in traction by wind.	
Fine regolith	Dusty, fine, and sand-size particles (~0.08 mm–0.53 mm) filling low areas between outcrops, locally covering outcrops, and in continuum with aeolian bedforms	Variable mixtures of autochthonous weathering, airfall dust, and aeolian sand transport	
Coarse regolith	Regolith dominated by coarser (1 to 2 mm) particles, frequently restricted to areas of several meters	Lag deposits resulting from wind stripping finer components in fine-grained regolith	
Mixed regolith	Poorly sorted mixture of angular rocks of various lithology between 2 to 20 mm in matrix of fine regolith and scattered coarse grains	Fine-grained regolith trapped in local relief and clustered rocks	
Float	Angular blocks and clasts (10 mm–<1 m) at base of escarpments capped by Ch and Ro	Slope debris associated with normal backwasting of resistant cap rocks	

Table 3
Continued

In situ map name/unit	Description	Field interpretation	Example from traverse
Crater ejecta	Angular blocks and clasts near rims of less eroded impact crater greater than 20 m in diameter	Ejecta excavated from local bedrock and regolith	

Fine regolith (map unit **r**) is uniformly fine (between ~ 0.08 – 0.53 mm), fills intervening areas in local relief and covering low-lying bedrock, and generally occurs as a continuum with surrounding aeolian bedforms. “Dusty” as used here refers to the fact that substantial dust-size material is mixed with measurable larger particles resulting in an otherwise dusty fine sand. *Coarse regolith* (map unit **rp**) consists of well-sorted grains (1–2 mm) distributed over areas several meters across or collected near the bases of boulders. *Mixed regolith* (map unit **rr**) is defined as a mixture of rocks between 2 and 20 mm set within otherwise fine regolith. Locally, the larger lithic fragments and angular blocks are derived from underlying or nearby rocky exposures of bedrock lithology. In addition to these dispersed bedrock fragments, near the landing site there are instances of distinct types of mixed regolith.

Aeolian bedforms (unit **a**) are one of the more pervasive regolith materials and are similar to those observed at meter-scales in other landing sites previously (e.g., Sullivan et al., 2005). This range in length from several centimeters long and a few centimeters wide often in association with local rocky obstructions to mega ripples 20 m long and 1–4 m (Sullivan et al., 2022).

Small impact craters/degraded impact craters. Approximately 16 small impact craters from 20 cm to 2 m in width are detected in regolith that is thick enough to bury bedrock along the traverse. These are featureless depressions, generally circular, and frequently clustered where they occur. Rims tend to be mixtures of fine and coarse regolith and are filled asymmetrically with fine regolith and ripples.

3.1.2. Bedrock Units

Outcrop scale observations of the principal identified lithomorphologies are summarized in the following with examples of each lithology in Navcam and Mastcam-Z and with macroscopic or “hand specimen” scale observations using Supercam RMI (Table 4). These type examples were used in defining the mapped lithologies in this paper. Differences in description and assigned identifying characteristics for each of these lithomorphologies suggested elsewhere (Horgan, Udry, et al., 2023; Simon, Hickman-Lewis, et al., 2023) lead to alternative stratigraphies and map unit distributions and account for some of the respective differences in stratigraphic interpretations along the traverse. Caution is warranted in relying on any single interpretation of the stratigraphy until some of these differences in lithomorphologies are better understood.

3.1.2.1. Máaz Formation

Perseverance landed near a rock later named “*Máaz*” subsequently identified as a recurring lithology. “*Máaz*” is a somewhat concentrically zoned, granular-appearing rock buried in regolith and exposed by the landing rocket scouring. The *Máaz formation* consists of a sequence of at least five lithomorphologies with mappable boundaries and overlapping relations, from the youngest to the oldest of which are *Ch'al member*, *Nataani member*, *Rochette member*, *Artuby member*, and *Roubion member*. Compositionally, the *Máaz formation* is distinguished principally by the near absence of olivine based on PIXL measurements in several locations together with the absence of distinctive olivine spectral bands in Mastcam-Z and MRO/CRISM compared with rocks in adjoining

Table 4

Field Image and Macroscopic Descriptions of Bedrock Lithologies in Panoramic and SuperCam RMI Images

Mááz formation^a

Cha'al member (map unit Ch)



Field Description: Rough, high relief, non-systematic jointing, vesicular angular massive blocks & crater-retaining plains

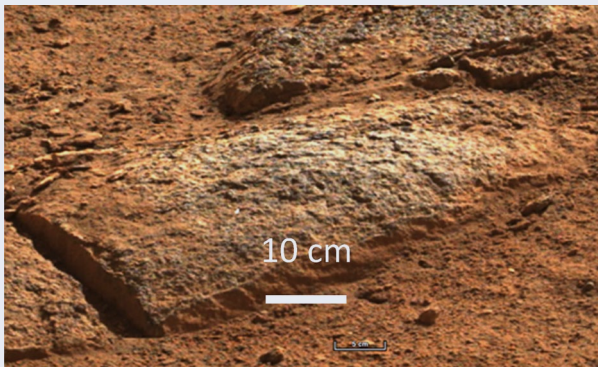
Field Interpretation: Aphyric coarse-grained basalt with aa-type lava sectional habit



Micro-Surface: Uniformly nubby surfaces; glossy surface luster on grains

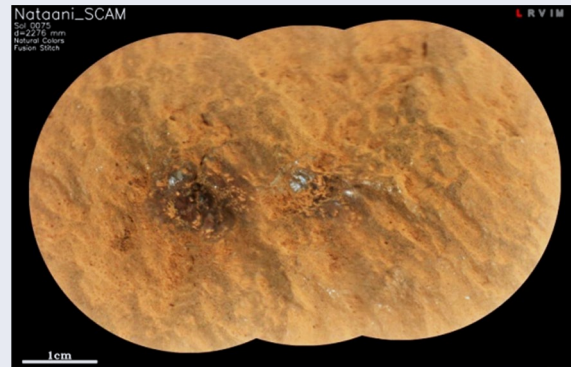
Petrographic Character: Isotropic, homogeneous, fine- to medium-grained crystalline (interlocking crystals)

Nataani member (map unit Nt)



Field Description: Coarse-grained, low relief surfaces with tortoise shell surface jointing at sub-meter scale; local dark vesicular protuberances

Field Interpretation: Diagenetically altered basaltic lithology, local weathering shells and core stone behavior and disaggregation halos of grus



Micro-Surface: Smooth—ridged; dull surface luster; local shiny, dark-toned, cm-sized patches

Petrographic Character: Splotchy, clotted coating; tightly packed, very fine to fine, round to egg-shaped “grains” that consist of a tiny dark-toned core wrapped in a light-toned exterior

Rochette member (map unit Ro & hRo)

Table 4

Continued

Mááz formation^a

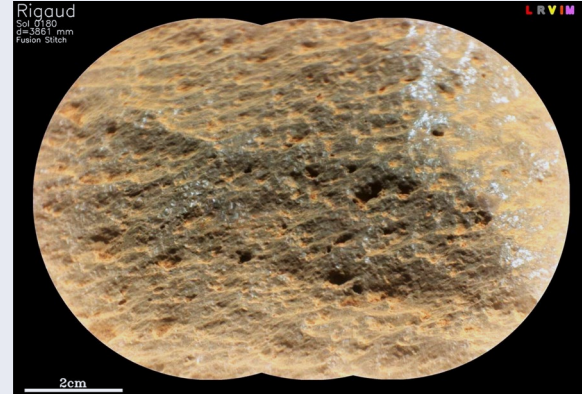


Field Description: Jointing, vesicular to scoriaceous basalt slabs; fissile sheets near basal contacts; dense interiors, and sub-polygonal outcrop exposures

Field Interpretation: Exhumed and well-preserved

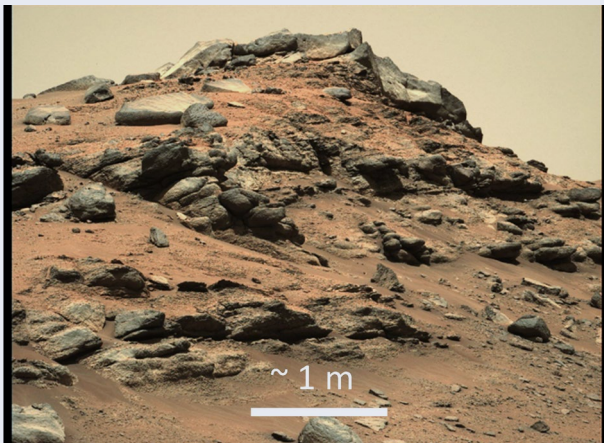
P-type basaltic lavas along eastern escarpment; slabby basal exposures capping Artuby Ridge

Artuby member (map unit Ar)



Micro-Surface: Evenly faceted, chatter marked (?); glossy surface luster not of primary origin

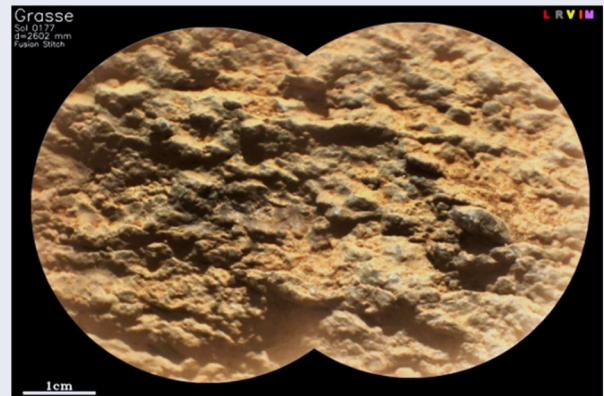
Petrographic Character: Medium-grained, crystalline rock; fine (mm) mesh-like pattern, possibly expressing a penetrative alteration of pyroxene and olivine crystals



Field Description: Ranges from foliated basaltic rock with horizontal vesicle tracks or sheets to coarse-grained, core stones with horizontal foliations yielding grus-like slope debris

Field Interpretation: Deeply weathered and altered basaltic rocks, (possibly sectional view of upper Roubion member?)

Roubion member (map unit Ru)



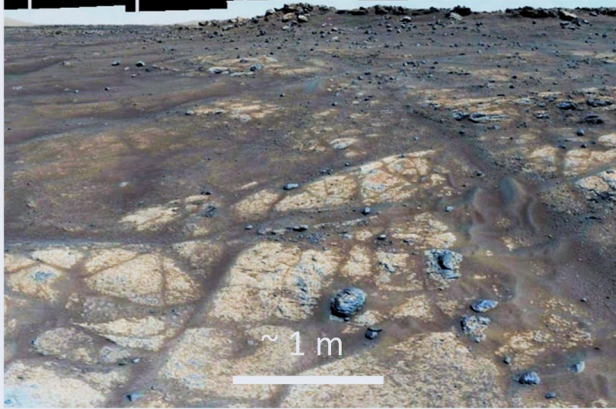
Micro-Surface: Unevenly grained, rough; dull surface luster

Petrographic Character: Layer-parallel fabrics; planar arrangements of tabular / platy cumulus minerals (mineral lamination)

Table 4

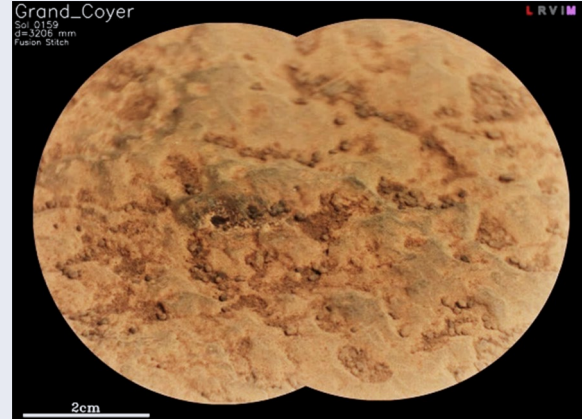
Continued

Mááz formation^a



Field Description: Coarse-grained, low relief surfaces forming benches near Mure; tortoise shell surface jointing at sub-meter scale, local dark vesicular protuberances

Field Interpretation: Diagenetically altered basaltic lithology, local weathering shells, core stone behavior, and grus disaggregation halos

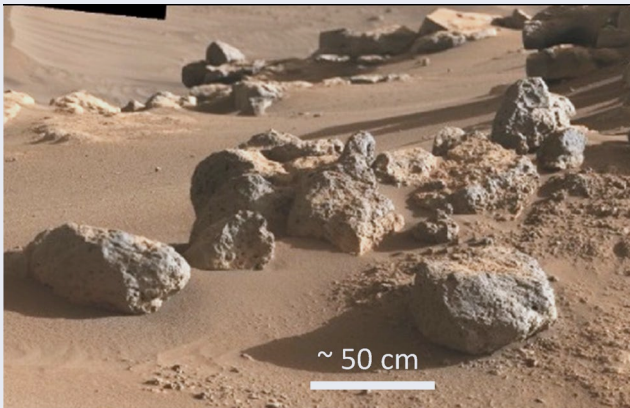


Micro-Surface: Smooth – pockmarked; dull surface luster

Petrographic Character: Splotchy, clotted coating; alteration texture, similar to Nataani member

Séítah formation^a

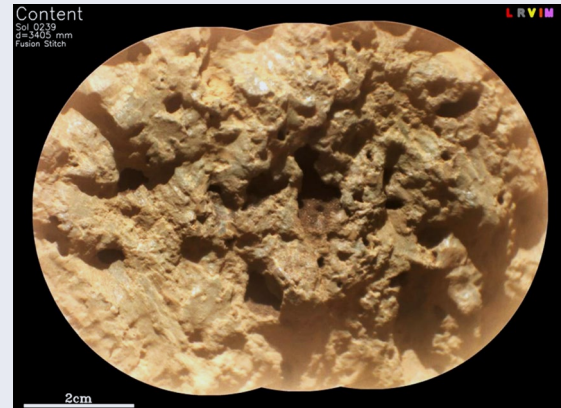
Content member (map unit Co)



Field Description: Sub-round vesicular blocks on the crests of Séítah ridges

Field Interpretation: Basaltic lava possibly unconformable with substrate

Séítah undivided member (or Issole member) (map unit S)



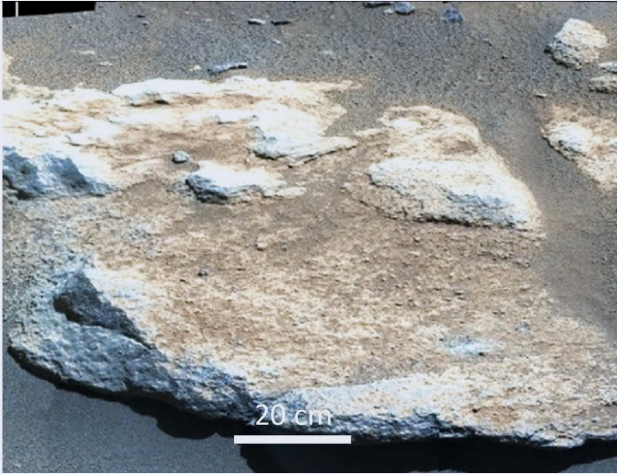
Micro-Surface: Rough - pitted (pits are dissolved and/or ripped off crystals; pits in some scattered rocks are circular and occur close-packed; dull surface luster)

Petrographic Character: Medium-grained igneous rock; euhedral, equant, dark-toned crystals, ~1-2 mm in size; mesh-like (subophitic?) texture

Table 4

Continued

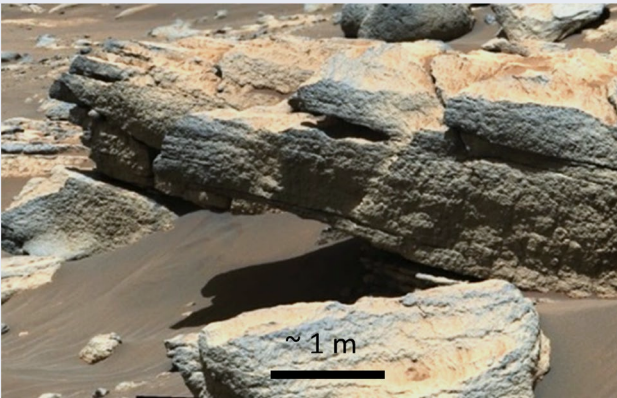
Séítah formation^a



Field Description: Thick slabs of coarse-grained material dipping SSE near base of Artuby Ridge slopes; includes the outcrop “Issole.”

Field Interpretation: weathered and altered mafic igneous rock mass, possibly the upper sections of cumulate rocks seen lower in the section at Brac-Caille members

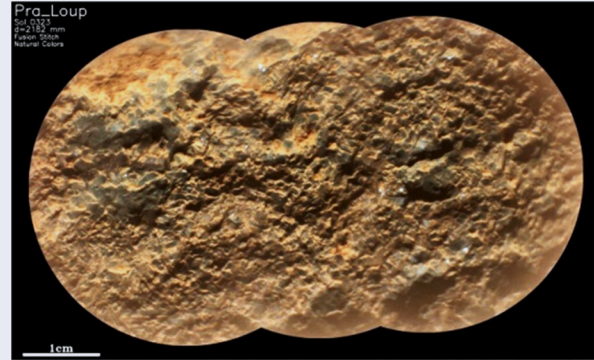
Caille member (map unit Ca)



Field Description: Dark fissile fine-grained outcrops defining Séítah ridges; dipping SSE

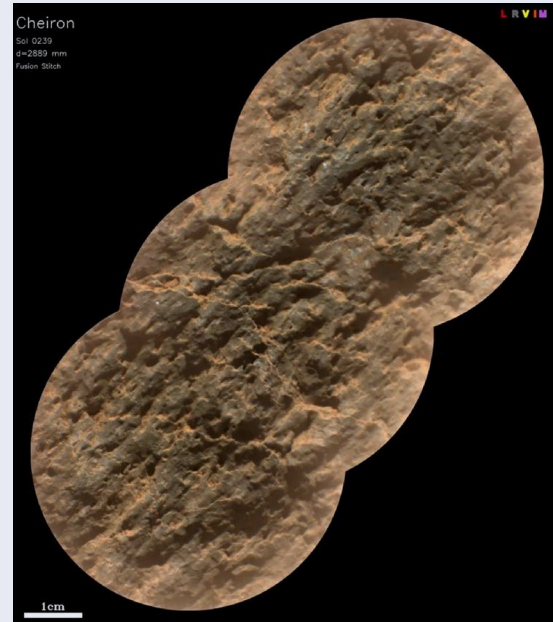
Field Interpretation: Olivine basaltic or gabbroic rocks

Bastide member (map unit Ba)



Micro-Surface: Unevenly grained, rough; glossy surface luster

Petrographic Character: Cumulate texture; arrangement of subeudral, cumulus olivine grains of fine - medium size

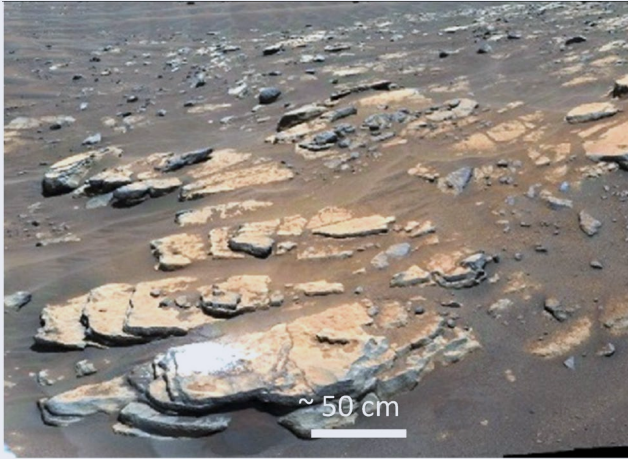


Micro-Surface: Uniformly grained – rough; dull surface luster

Petrographic Character: Granular (cumulate?) texture; aggregation of mineral grains of ~ equal size (medium grains)

Table 4
Continued

Séítah formation^a



Field Description: Platy, slabby light-toned and coarse exposures in slopes of Séítah ridges dipping SSE

Field Interpretation: Deeply weathered cumulate olivine basaltic or gabbroic rocks transitional between Issole and Caille members.



Micro-Surface: Evenly furrowed; dull surface luster

Petrographic Character: Layer-parallel fabrics; planar arrangement of tabular / platy minerals with cumulate texture (mineral lamination)

Note. Petrographic descriptions are field or hand specimen descriptions and serve only to highlight the characteristics that were identifiable in specimens examined in the field. The degree of detail provided accordingly varies from sample to sample as a result of variable exposure and preservation in each outcrop.

^a*Máaz formation* is equivalent to Cf-fr and *Séítah formation* is equivalent to Cf-f-1 photogeologic map units of Stack et al. (2020).

areas such as Séítah. This is fundamental distinction applied in the “field” by the team stratigraphic model and is used to define the contact between *Máaz* and *Séítah formations*.

Ch'al member occurs as a terrain retaining eroded impact craters (Calef et al., 2022). In the type locality, a rock named “*Ch'al*” ~60 m from the rover on sol 68 consists of dark, massive blocky (sub-to meter-scale) and elevated rocks bearing scattered pits. The pits are interpreted as likely vesicles on the basis of the fundamental igneous petrologic nature of the rock and its lava sheet-like occurrence across the crater floor. Orbital data indicate that this rock unit extends east of the landing site across the crater floor for at least several kilometers.

Based on RMI observations of the rock matrix between vesicles and with proximity instruments of target rock “*Sid*” (on sol 362), *Ch'al* is a medium-grained (1–3 mm) rock with interlocking crystalline grains indicative of an igneous texture and is a relatively alkaline composition (trachybasaltic to trachyandesitic) (Schmidt et al., 2022). The summary interpretation is that these rocks are likely evolved basaltic lavas (Farley et al., 2022) in which the complex fracturing and angular polygonal shapes in the outcrop arose from normal strains occurring within solidifying lava and post-emplacement impact processes, followed by later erosion of the finer scale upper lava textures on the surface.

Nataani member is one of the more extensive *Máaz formation* lithologies and is characterized from orbital images by a relatively low-lying surface distinctly textured in polygonal patterns. In Perseverance Navcam and Mastcam-Z images, exposures of the Nataani member were characterized by low relief (centimeters) fractured-bounded margins arranged in sub-polygonal patterns. In initial Mastcam-Z images, the rocks have notably coarse, granular (1–3 mm) surface textures near the landing site with accumulations of gruss around

their margins. Many exposures preserved evidence of concentric foliations grading inward to more coherent rock analogous to spalling “corestone” morphology that envelops blocks of severely weathered and fractured but otherwise uniform rock masses. Many local exposures are populated by pits 2–5 mm in diameter, interpreted as larger vesicles that frequently occur in the massive interiors of lava. Although in this case, if the rocks were initially emplaced as lava, the granular and crumbling character, specifically the gross identified around individual polygons, suggests a substantial alteration. Eastward from the landing site and closer to the contact with the overlying *Cha-al member* the surfaces of *Nataani member* exposures are characterized by dark protuberances that in the type location, a target named “*Nataani*” (Sol 68 contact science analysis), appear to grade downward without compositional distinction based on Mastcam-Z multispectral observations into the more granular underlying rock face. The contact with the overlying and high relief *Ch'al member* exposures was not directly observed.

Supercam RMI observations further identify somewhat oblate grains up to 1 mm with darker cores within a lighter matrix, also suggestive of substantial alteration of an original mineralogy. The summary interpretation is that these are deeply altered igneous rocks of undetermined protolith.

Rochette member lithology occurs 60 m outward to the south from the escarpment bounding Séítah on the east and may be more widespread south of its occurrence capping Artuby Ridge as isolated rocky hummocks (map unit hRo). Where large exposures occur, the outcrops are sub-orthogonally jointed and locally scoriaceous exposures grade downward into dense aphanitic-appearing masses. Several curvilinear vesicle sheets are notable in the outcrop and are conformable to the elliptical overall shape of the denser parts of the outcrop. In the type location, a tabular prismatic block selected for the first successful core sample, the Rochette lithology is a dark, dense, and pitted pyroxene basalt capping Artuby Ridge (Simon et al., 2021).

Supercam RMI images of *Rochette* are characterized by ~1–2 mm pits interpreted as vesicles, crystalline grains 1 mm and less, and rough sub-parallel linear fabric of rougher grains aligned with local vesicle elongations. The Rochette lithology is interpreted as a basaltic lava flow based on the combined mineralogy and elemental abundances from proximity science observations and the apparent increased abundance of pits near the top of outcrops typical of vesicles in the upper sections of basaltic lavas.

Artuby member is exposed as distinctly foliated outcrops underlying the contact with *Rochette member* basalt and overlying *Roubion member* exposures. At Mure, the exposures display centimeter scale sheets and fissile layers of coarse 1–3 mm granular material immediately underlying Rochette cap rocks. Elsewhere along the slopes of Artuby Ridge, these grade downward to lens-shaped grussy outcrops with a corestone-like or concentrically foliated appearance.

In RMI data, *Artuby member* lithology is granular with elongate tabular and platy grains averaging 3 mm or larger generally arranged in a linear fabric consistent with outcrop foliations typical of Artuby exposures in general.

The interpretation of *Artuby member* rocks is unresolved by the observations. These are rock masses that have been highly altered, but the protolith is undetermined and the sub-horizontal foliations and overall appearance of layering are not easily understood in the context of the in situ examination of structure and mineralogy. They could be foliated igneous rocks or the result of a sedimentary process.

Roubion member outcrops are physically similar to *Nataani*, consisting of low-lying polygonal exposures with granular surfaces, dark protuberances in proximity to the overlying caprock of *Rochette member*, and orthogonal patterns of local fractures defining polygons. The principal distinction is its location west of an apparent *Rochette member* cap rock, and its lower elevation by ~10 m.

RMI data on Roubion are similar to *Nataani member*. *Roubion* has a surface that is rough at centimeter scales bearing slightly darker grains in a lighter matrix. The fabric as defined by these “grains” is roughly linear. Dark, circular 1-cm-diameter pits are notable in one Watson image. No circular mineral phases or clasts are noted that could have been removed during surface exposure and erosion, so the field interpretation is that these are large and widely dispersed vesicles in the otherwise uniform rock mass, although the possibility remains open that these are a form of dissolution pit based on the host rock's alteration.

The *Roubion member* is interpreted as representing a similar, but unconstrained, protolith as the *Nataani member*. It is possible that the *Roubion member* is a lower expression of *Nataani* in which Rochette has been disconformably emplaced as part of the sequence.

3.1.2.2. *Séítah Formation*

Séítah is a hilly terrain of isolated outcrops engulfed by abundant float and scree, and is regionally elevated. The prevalence of aeolian bedforms limits continuous exposure of bedrock mostly to hill slopes and summits. The determination of lithologies here is based on only a few distinct outcrop expressions identified in the moat-like depression between *Máaz formation* and *Séítah formation* and within a 10 m high hill (“*Caille*”) 140 m northeast of Artuby Ridge during the acquisition of cored samples at the outcrop “*Brac*.” A principal characteristic of the *Séítah* region identified in pre-landing remote sensing was strong olivine spectral signals. In outcrops, olivine was confirmed in contrast to the rocks of the *Máaz formation* as well as significant foliations, slabs, and grain-size variations characterizing outcrops.

Content member lithology occurs as a capping of sub-round vesicular basaltic rocks near the crest of the visited *Séítah* Ridge. In RMI images, some pits do occur from apparent dislodging of crystals, but the circular aggregated pits and knobby surface textures are more typical of vesicular textures. Local clusters are fragmented blocks, sub-round in shape and are either resting on a former planar unconformity or preserved as resistant material following erosion of underlying rocks within *Séítah*. In situ remote sensing suggests that in contrast to most of the lithologies in *Séítah* olivine is not present in the *Content member* (Wiens et al., 2022), a characteristic more typical of *Máaz formation* rocks than *Séítah formation*. Because of the limited occurrence of these rocks, interpretations are varied. The occurrence of an unconformity and mineralogical distinction from the underlying *Séítah* rocks is interpreted by some to represent a lava flow origin. Others suggest that it is a sill. Either emplacement is consistent with the apparent vesicular and rough scoriaceous textures of some blocks.

Séítah undivided or Issole member includes a collection of continuous layers or foliations in coarse-grained outcrops along the base of the slopes leading up and southeast to Artuby Ridge. From a distance of several meters, the outcrops appear similar to Artuby and are distinctly foliated at 10-cm scales and less. Proximal examination and RMI images identify distinct 1 mm interlocking crystals supported in amorphous matrix bearing cumulate textural characteristics. At all scales examined, the exposures are foliated parallel to the larger scale layering and foliation that is typical of all the exposures within *Séítah*.

Caille member exposures occur along the crest of a *Séítah* hill named “*Caille*” and are approximately one m thick, dark, and foliated or layered materials with blocky weathering habits. From stand-off distances of more than several meters, the outcrops appear fine grained and distinctly layered at sub-centimeter scales. Higher resolution inspection with RMI identifies an overall linear fabric of dark angular 1 mm grains and a mineralogy consistent with a basaltic (gabbroic, if it is intrusive) composition.

Bastide member exposures at the base of the visited hill within *Séítah* are generally light toned and weather to slabby and tabular plates on local slopes. While appearing granular as with other *Séítah* exposures, the megascopic character is distinctly coarse with grains or subhedral dark crystals and distinct laminar textures throughout indicative of a cumulate origin. RMI observations are unusual in that the crystals are larger, 1–2 mm in size and are not obviously arranged in a linear or laminated fabric as with other *Séítah* exposures examined.

3.2. GXM Maps: Narrative of Mapping Observation Along Traverse

The following summarizes the observations made from successive locations along the traverse (summarized in Table 2) and highlights the macroscopic (“lithomorphologic”) characteristics that support mapping from the rover perspective, including physical characteristics, structural features, and relevant map relations. Locations of each map discussed in the following and general terrain characteristics are shown in Figure 5.

The location of the “*Octavia E. Butler (OEB) Landing Site*” approximately 1 km southeast of the Jezero crater delta front provided an opportunity to characterize the geologic context of the crater floor and relevant stratigraphic relationships before exploration of the delta. An important part of that effort includes the initial “crater floor campaign” (Sun et al., 2022) following a traverse to the south and along the contacts between two distinctive terrains (Cf-f-1 and Cf-fr) identified in pre-landing photogeologic mapping (Stack et al., 2020).

3.2.1. *Octavia E. Butler Landing Site Segment, Sols 001–105 and 355–358*

Summary Field Interpretation of the OEB Traverse Segment. This is a relatively low-relief segment of the traverse (Figure 6) confining mapping mostly to Level 3 (30 m). Mapping provided insights into two of the more extensive

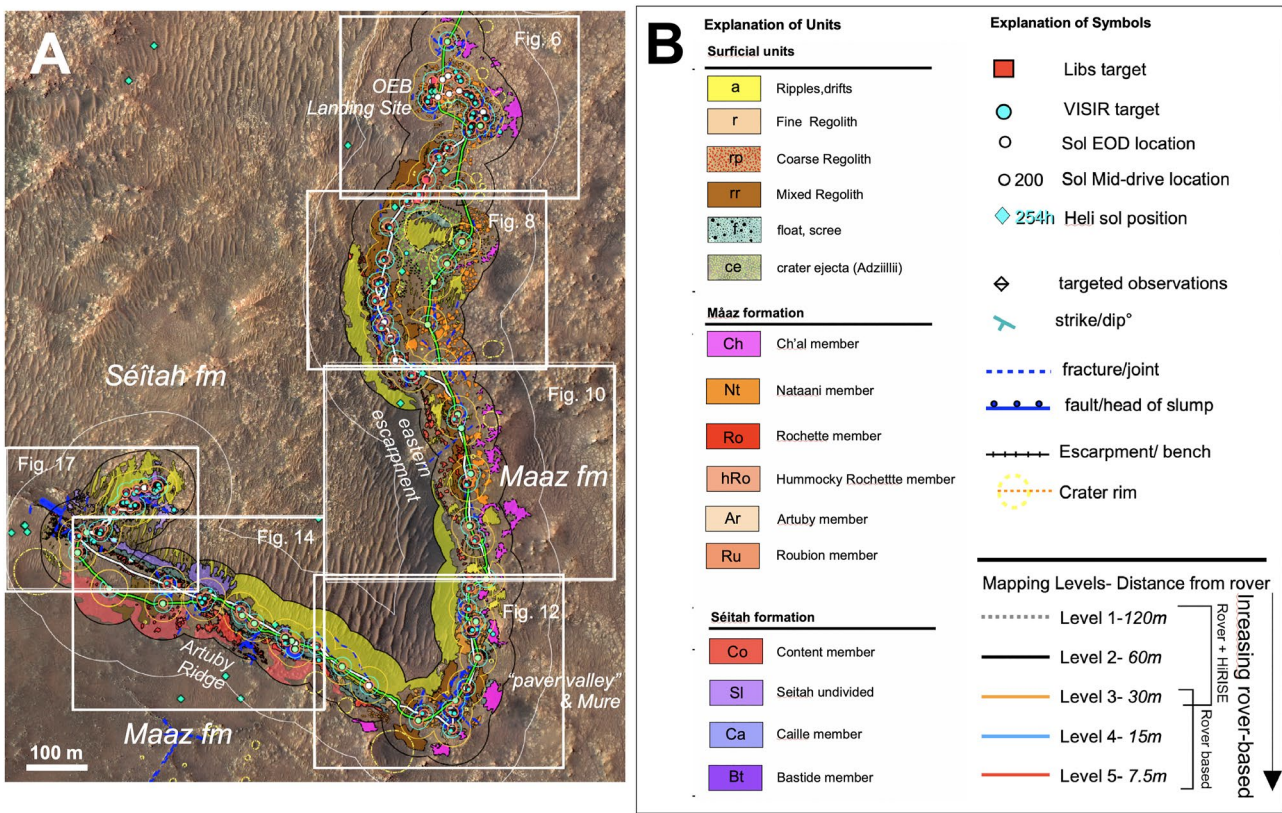


Figure 5. (a) Location of six quadrangle divisions within the final geologic context mapping map and discussed in Section 3. The dashed line identifies an escarpment that is also the approximate contact between the *Séitah formation* and *Máaz formation*. The base image is a Mars 2020 MRO/HiRISE mosaic. Concentric circles around each sol location indicate Levels 1–5. This and the following maps are in “Jezero Crater projection.” (b) Explanation of units in this overview and the maps (Figures 7, 9, 11, 13, 16, and 18) below.

lithologies on the crater floor, *Nataani member* and *Ch'al member*. Judging from the core stone type weathering enclosed in uniform polygonal joints throughout the low relief segments of this area, the *Nataani member* is a deeply altered and uniformly massive bedrock of undetermined protolith. Initial proximal science results at the target “*Nataani*,” significant exfoliation along joint boundaries, and deconvolution of spectra from SuperCam LIBS observations (Udry et al., 2023) suggest substantial chemical alteration of the original mineralogy.

Observations in this traverse segment also support *Ch'al member* rocks as stratigraphically overlying *Nataani members*. It is unclear if there is an unconformity between the two. The deep weathering along joint faces within the *Nataani member* and absence of similar alteration on the sharp edges of irregular joints in *Ch'al member* blocks support longer exposure of the *Nataani member* to weathering and alteration. This in turn could imply a significant time interval between *Nataani* and *Ch'al members*. It is also possible that erosion removed the upper zones within an original *Nataani member* lithology prior to the emplacement of *Ch'al*, accounting for the relatively flat-lying surface of *Nataani member* exposures.

The massive character, irregular jointing, and overall absence of strong vesicle zonation in Mastcam-Z images noted in *Ch'al member* boulders are more typical of aa type lava than pahoehoe (Macdonald, 1953; Self et al., 1998). This interpretation must remain tentative because the *Ch'al member* is broken and overturned, and a complete section necessary for confirmation of the aa characteristic flow structure typical of aa-type behavior has probably not been observed.

Overview of the Traverse Segment. Perseverance spent the first 100 sols investigating the vicinity of the landing site (Figure 5) located within the Cf-fr (crater floor-fractured, rough) pre-landing map unit, now called the *Máaz formation*. An operational focus of these first sols was the deployment of the Ingenuity helicopter and activities supporting documentation of the first attempted flights requiring traversing to the east approximately 60 m (sols

OEB Landing Site/ Sols 001 - 105; 360 - 379

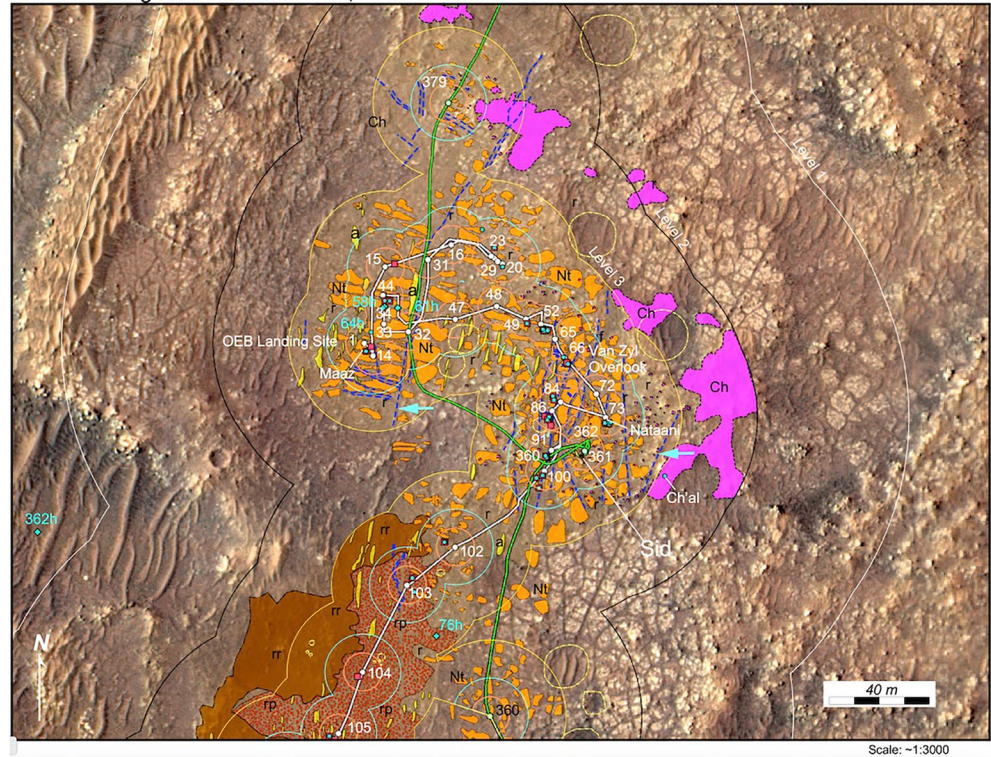


Figure 6. Geologic context mapping in situ geologic traverse map from sols 001–105, 360–379. Map units as in Figure 5 (White lines, inboard traverse; green lines, outboard traverse.) Arrows identify examples of long, through-going curvilinear fractures.

14–29), followed by a return to the vicinity of the landing site (sols 31–46), before traversing eastward again to the “Van Zyl Overlook” observation point (sols 47–64) in preparation for the documentation of the first flights of the *Ingenuity* helicopter. Science observations were interspersed throughout the traverse activities associated with those operations during the corresponding “walkabout.”

Lithomorphologies. Two bedrock lithologies bearing distinctive visual mappable characteristics are identified in the vicinity of the landing site (Table 4): Centimeter-relief, light-toned, granular textured outcrops arranged in a dispersed polygonally jointed pattern, presenting the appearance of “paver stones,” and elsewhere referred to as such, in their nearly flat surfaces and systematic arrangement (*Nataani member*) (Figure 7a foreground, Figure 7b); and angular, dark gray and fine-grained rocks clustered in a high-standing rise to the east (*Ch'al member*) (Figure 7a background), Figure 7d). The intervening areas between polygons (*Nataani member*) are filled with fine (unit r) to coarse (unit rp) regolith and local aeolian ripple bedforms. Isolated rounded cobble-sized vesicular materials occur within the regolith in many scenes, but pebble-sized lithic clasts are more common.

The angular, dark gray and fine-grained rocks clustered in higher-standing rise to the east (*Ch'al member*) are western margins of an extensive rough crater floor covering unit in HiRISE images that retain more craters than elsewhere on the crater floor. These lie above the *Nataani member* polygonal-jointed outcrops throughout the traverse. The contact between *Nataani* and *Ch'al* members is not observed, although several *Mastcam-Z* panoramas show that the transition must occur abruptly at the base of *Ch'al member* outcrops, generally obscured by the float from *Ch'al* outcrops (Horgan, Rice, et al., 2022). The boulders of the *Ch'al member* that defines the main outcrop masses are up 1–2 m, frequently pitted with curvilinear fracture surfaces and sharp edges at non-orthogonal intersections of joint faces. This is distinctly unlike the more orthogonal jointing noted elsewhere in dense dark rocks such as *Rochette member* rocks seen farther along the traverse. Proximity observations of elemental chemistry on a boulder of *Ch'al* (“*Sid*”) during sample acquisition (Wiens et al., 2022; Simon, Hickman-Lewis, et al., 2023) indicate that *Ch'al* has intermediate igneous composition with relatively high silica

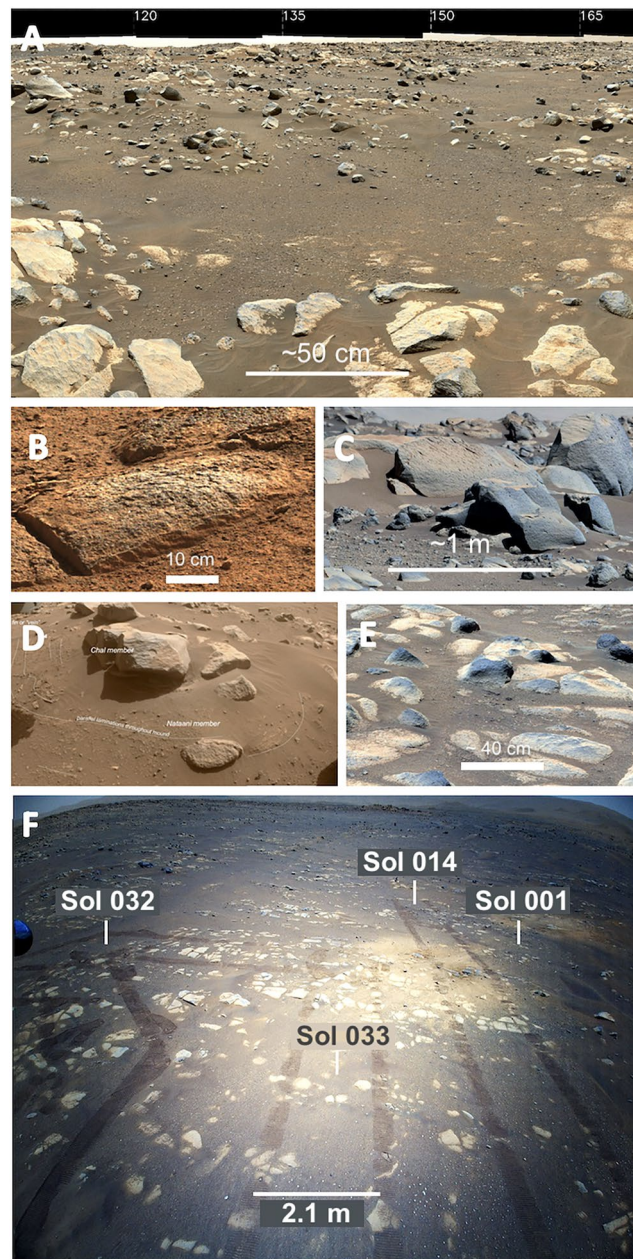


Figure 7. (a) East-southeast-directed view from the sol 78 location of the approximate area of contact between polygonally jointed outcrops (*Nataani member*) and dense clustered overlying blocks (*Ch'al member*) in the distance. Azimuths from rover position indicated at the top of image. QZCAM_Sol078_ZCAM08039_L0_Z034_Landing_Site_E1. (b) Approximate southeast-directed view from the landing site of a granular polygon with exfoliated margins (the rock, *Máaz*) typical of *Nataani member*. ZRF_0003_0667218910_000FDR_N0010052AUT_04096_034085J01 (c) Southeast directed view of the type location (*Ch'al*) for dense, sparsely vesicular clustered boulders 1–2 m in width with curvilinear fracture margins. The massive character, near-absence of vesicle zonation, and abundant scoriaceous litter near the base of the outcrops are typical of aa lava sections on Earth. QZCAM_SOL0078_ZCAM08041_Z110_L0_EE_SCL_CYL_CHAL_BOULDER_01 (d) South-directed view from the sol 371 location of *Ch'al member* sample target *Sid* (~55 cm wide) resting on a pedestal consisting of eroded *Nataani member* lithology. Hazcam image FRF_0371_0699886528_941FDR_N0110108FHAZ02008_0A00LLJ02 (e) Southeast-directed view from the sol 78 location of dark protuberances on the upper relief of individual polygonally jointed *Nataani member* exposures proximal to the *Ch'al member* exposures. QZCAM_SOL0078_ZCAM08039_L0_Z034_DIBAHI_NATAANI_LANDSCAPE_E1 (f) Ingenuity color camera southward-directed view of polygons or “pavers” in the vicinity of the *OEB Landing Site* (identifiable by the paired bright rocket-scoured surfaces on the right) acquired on sol 64, Flight 3. Rover track is approximately 2.7 m wide (HSF_0064_0672622186_471FDR_N0030001HELI00000_000085J02).

and high alkalis, and that it is one of the more evolved igneous rocks encountered (a trachyandesite in the total alkali-silica igneous rock classification).

Throughout the walkabout from *OEB* to the *van Zyl Overlook* area, small vesicular cobbles occur in the regolith between polygons and increase in occurrence with proximity to the *Ch'al* outcrops. Isolated dark, massive textured boulders and cobbles bearing lithologies comparable to the *Ch'al member* are scattered in diminishing numbers westward toward the landing site, often directly resting on *Nataani member* polygonally jointed outcrop surfaces. One of these boulders, “*Sid*,” was sampled at the end of the crater floor campaign where it rested on *grus*-like exposures of *Nataani members* bearing horizontal laminations or foliations (Figure 6d). It is unclear if this is a contact or if the *Ch'al member* boulders are simply float or residual outliers of extensively eroded *Ch'al member* bedrock perched on eroded *Nataani member* bedrock.

Dark upper relief surfaces and protuberances were characteristic of *Nataani member* outcrop polygons, particularly within ~50 m of the *Ch'al member* exposures (Figure 7e). Based on SuperCam remote laser-induced breakdown spectroscopy tracks on at least one example, these are similar in composition to *Nataani member* exposures farther west. The transition between the protuberances and underlying polygons is gradational and appears to be coherent with no obvious contact. Many of these dark protuberances are difficult to distinguish from isolated and scattered blocks of *Ch'al members* occurring as outliers from the principal unit to the east.

From sol 102, the traverse passes southward through a region of abundant regolith and only scattered float consisting of miscellaneous aphanitic dark rocks with abundant ventifacts (Herkenhoff et al., 2023). A low rise or bench to the west of the traverse consists of blocks engulfed in regolith (unit **rr**, mixed regolith), a characteristic observed sporadically along the traverse in areas between the escarpment to the west bounding *Séítah* and the crater floor units and polygonally jointed terrain along the traverse. Between sols 103 and 105 locations and abutting the mixed regolith on its east margin is usually a large (tens of meters) area of coarse regolith (unit **rp**, coarse regolith). Because this area is depleted in aeolian bedforms, implying a net deficiency of sand supply (trapped in the mixed regolith to the immediate west?), the coarse regolith here may be a lag resulting from aeolian scoring of the fines (sand) typical of regolith observed elsewhere along the traverse. *Nataani member* polygons emerge from this zone of widespread regolith approximately 40 m to the east of the pebbly regolith area along the traverse on sol 360 during the return northward. The traverse between sol 102–105 appears to cross a zone of deep regolith accumulated within a broad low-lying area inboard of the escarpment bounding *Séítah* and locally burying the bedrock lithologies and regional fractures.

Structural Characteristics. *Nataani member* outcrop polygons tend to be grouped or arranged in gregarious sets bound by approximately orthogonal joints and intervening regolith. Within the gregarious sets, individual polygons are defined by relatively straight joints and somewhat rounded corners along the margins of polygons although in a few places they approach circular shapes. The shape of the polygons and polygon sets varies systematically from west to east across the part of the traverse (Figure 7f). West of the *Van Zyl Overlook*, the shapes of the low-lying polygonal outcrops are elongated (length to width ratio, 2.0), the long axis striking N98°E with intervening regolith zones 1–1.5 m wide, and generally equant farther eastward and southward. Sixty to 70 m to the east of the landing site, beginning at the *Zan Zyl Overlook*, the polygons are more closely spaced (6–8 m), more equant with approximately northeasterly striking orientation through-going regional fractures. The change in the aspect ratio of polygons and the spacing of regional through-going fractures is gradational and occurs over a gentle rise in the terrain eastward.

Larger, roughly parallel, through-going fractures are prominent throughout the crater floor where polygonally jointed outcrops occur (Figure 6, long fractures). Although regionally sweeping in arcs, these tend to be approximately parallel to the boundary between the *Séítah* terrain and the surrounding crater floor units. A single through-going fracture 60 m long striking roughly at right angles (North to N7°E) to the elongation axis of the individual polygons occurs near the landing site, where the polygons are somewhat more elongated. Farther southward fractures become less apparent as the surface is dominated by increasingly more regolith and fewer outcrops along the traverse.

3.2.2. Adzilli Crater and East *Séítah* Margin Traverse Segment, Sols 105–128 and 355–359

Summary Field Interpretation of Adzilli and East *Séítah* Margin Traverse Segment. Large areas of regolith and isolated exposures of *Rochette members* characterize much of this traverse segment. The return northward trav-

East Séitah Margin Escarpment / GXM Sols 105 - 128; 355 - 358

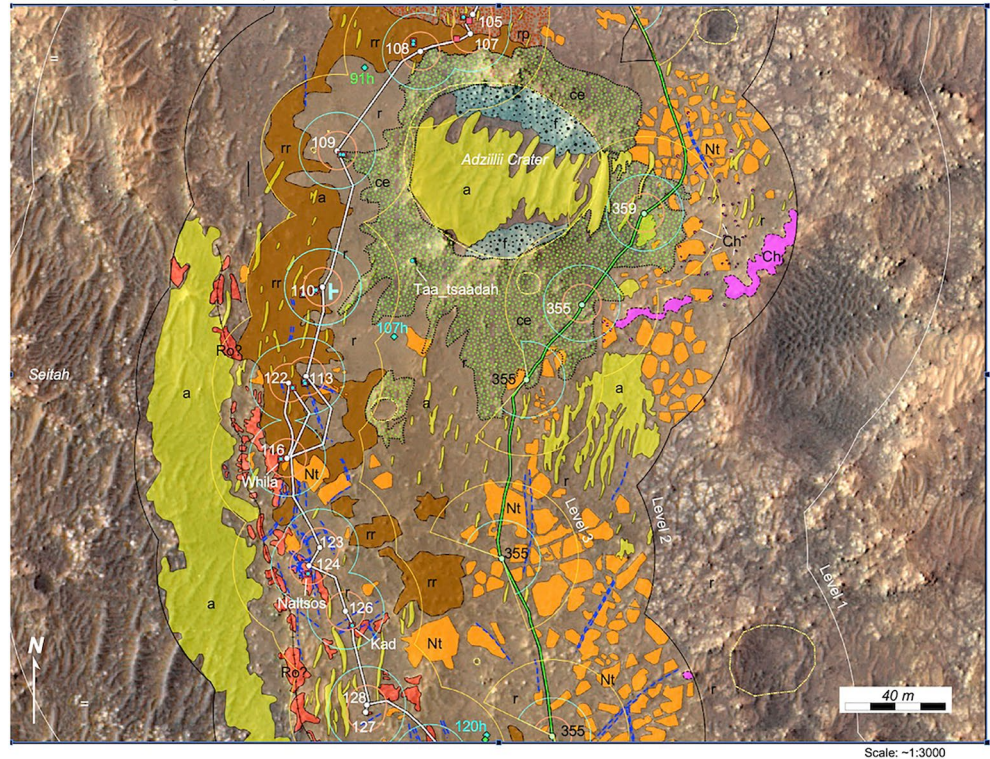


Figure 8. Geologic context mapping in situ geologic traverse map of the Adzilli-East Séitah Margin Traverse Segment from sols 105–127 and 355–358. Map units as in Figure 5 (White lines, inbound traverse; green lines, outbound traverse).

erse encounters *Nataani member*, ejecta from *Adzilli Crater*, and a slender outlier of *Ch'al* (Figure 8). A lithology observed for the first time in the southward-traversing segment includes probable basaltic outcrops identified as *Rochette member*; gradients in vesicular textures and planar surface chill zone morphologies, generally scoriaeous textures, and orthogonal block shapes typical of the near upper surface of typical pahoehoe type lavas are a characteristic that makes *Rochette member* distinctive and identifiable in panoramas as distinct from irregularly jointed, blocky and massive *Ch'al member* outcrops in which vesicles are less abundant at macroscopic scales. The preservation of original basalt surface texture in the vicinity of the escarpment bordering Séitah and possibly in the ejecta of *Adzilli crater* is consistent with the westward up-dip projection to the surface of a dense reflector in RIMFAX data and the exposure of that dense reflector along the eroded escarpment by exhumation. Because the stratigraphic sequence also steps from older to younger eastward, the observed easterly dip appears to be a regional characteristic along this part of the traverse.

Overview of the Traverse Segment. On Sol 105 Perseverance arrived at the north side of Adzilli Crater, a ~75 m-diameter impact crater with a rim of blocky debris 6 m high and traversed through Sol 110 around the west margin of the ejecta in a trough of filled with fine regolith bordered on the west by coarse regolith. On Sols 110–113, the traverse was within 30 m of the escarpment bounding Séitah on the west where the outcrops were identified as dark and vesicular blocks. This was examined on Sol 116, followed by a 40 m traverse northward to test Autonav, an autonomous driving technology. All subsequent drives along the traverse route were correspondingly extended using Autonav compared with previous traverse segments. Drives southward followed the contact between polygonally jointed granular lithology (*Nataani member*) and a new lithomorphology consisting of dark, vesicular rocks inboard of the escarpment bounding Séitah.

Lithologies. Distinct lithomorphologies differing from those at the landing site were exposed both in the ejecta of *Adzilli crater* (Sols 107–110) and near the escarpment along Séitah to the west between Sols 113–129. The rim ejecta of the Adzilli crater consists of dark, dense, and mostly angular blocks (Figure 9a). Many of the more rounded blocks are characterized by close-packed vesicles. Individual vesicles cannot be resolved although the

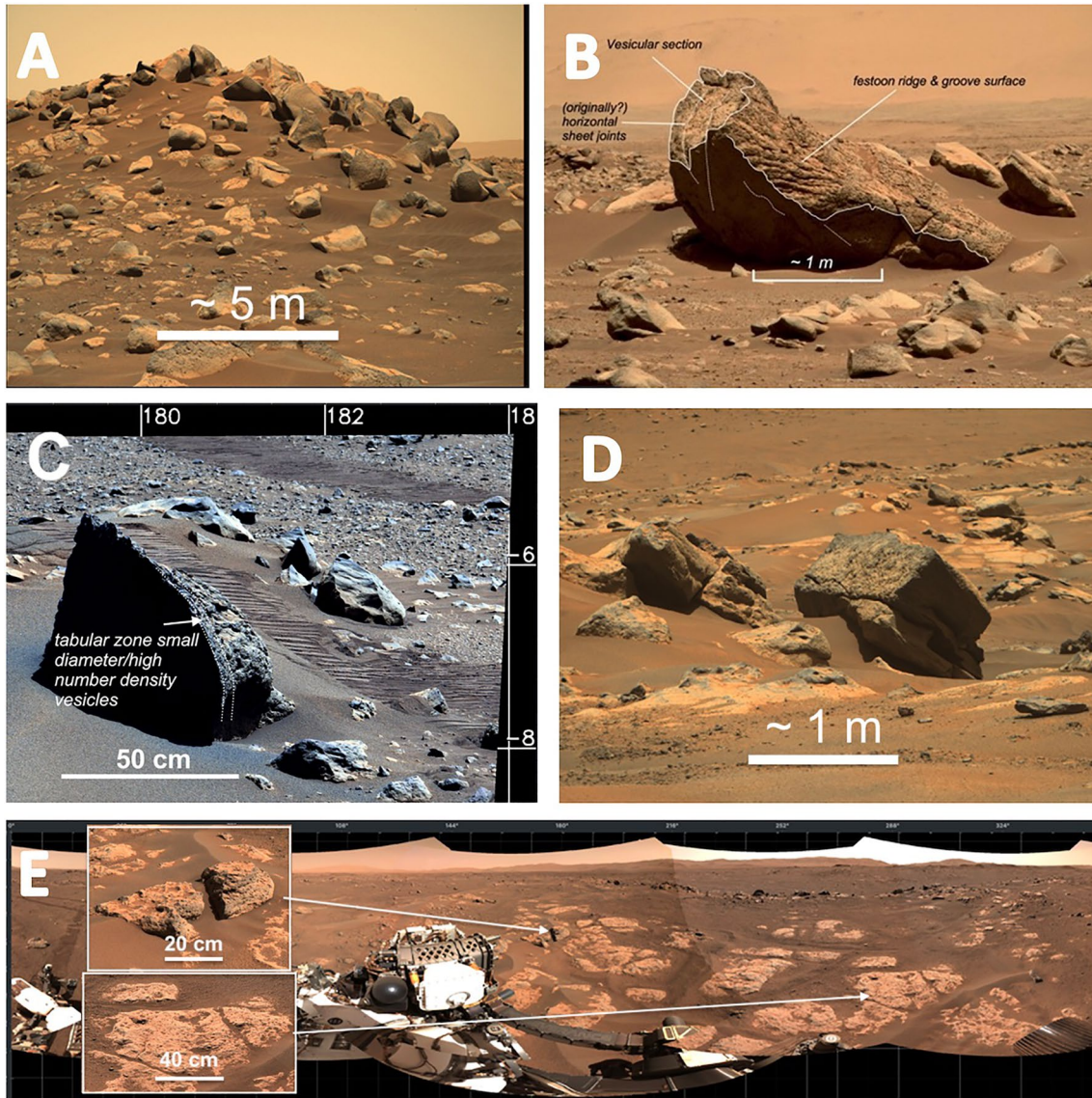


Figure 9. (a) Eastward-directed view of lithomorphologic mapping characteristics of *Rochette member* rocks exposed in the ejecta of Adziilii Crater and along the traverse near the escarpment bounding Séítah. Image ZRF_0109_0676616059_644FDR_N0040738ZCAM08080_0340LMJ02 (b) *Taa_tsaadah*, an unusual block in the ejecta of Adziilii Crater bearing surface festoon ridge and groove morphology and interior vesicular section, and originally horizontal joints representing sutures between vesicle zone layers. East-northeast-directed view from sol 110 location. ZRF_0110_0676704984_053FDR_N0040822ZCAM03159_1100LMJ04 (c) Up-ended slab of vesicular basalt characterized by a vesicle sheet and planar textures typical of pahoehoe lava. View south from sol 122 location. Image acquired at sol 122 location on sol 123 before drive. Azimuth and altitude in degrees from rover position on top and right. ZRF_0123_0677861106_225FDR_N0041422ZCAM08119_1100LMJ01 enhanced-color image. (d) Westward-directed view from sol 124 location of block cantilevering toward Séítah along the marginal escarpment showing a cross section of a near-surface basalt vesicular zone. Note the greater number density of vesicles relative to the underlying horizontal surfaces of outcrops in the surroundings. Image ZRF_0124_0677947815_269FDR_N0041644ZCAM08121_1100LMJ0. (e) Dense planar surfaces bearing scattered cm-size vesicles and orthogonally jointed arrangements of outcrops. Insets identify vesicular upper surface rubble and cm-sized vesicle pits on orthogonal planar upper faces typical of the middle to upper interiors of inflated basaltic sheet flows. South-centered 360° panorama N_LRGB_0124_RAS_0041712_CYL_S_CLRREPRJ01.

texture is rough and scoriaceous-appearing at scales of several millimeters or greater. These rocks contrast with the dense, dark, angular blocks noted in the *Ch'al member* to the east of OEB Landing Site, particularly in that the larger, texturally massive rocks are defined by fracture faces somewhat less curvilinear than the *Ch'al member* exposures.

One 2 m × 1 m block on the southwest slopes of the rim ejecta ("*Taa_tsaadah*," Figure 9b) is characterized by abundant vesicles on one narrow face and long, festooned 0.5–1 m long grooves on the long upper face. Several

origins are considered for this unusual morphology, including ventifacts and preserved basaltic ropy structures.

The return traverse on Sols 355 through 359 skimmed the thin east margin of the *Adzillii crater* ejecta, where it is largely covered by regolith and overlies the *Nataani member* polygonally jointed outcrop, passing near the west-southeastward extended ridge of *Ch'al member* dark angular blocks at the Sol 355 end-of-drive location.

Southward from the sol 110 location on the west side of *Adzillii crater*, the traverse followed a trough of regolith several meters wide and bordered on the east by scattered outcrops of polygonal-jointed *Nataani member* rocks 30–40 m distant and poorly resolved. This identification is supported by near-field mapping in the return traverse observations on sol 355 80 m to the east.

To the west from sol 116 to 128, distinctly dark and vesicular rocks occur in scattered outcrops inboard from the Séítah bounding escarpment and eastward to 30 or 40 m. Outcrops and isolated rocks at the sol 116 (*e.g.*, *target Whila*), sol 122, and sol 124 sites (Figures 9c, 9d, and 9e). Vertical gradients in vesicle size and abundance in vertical sections observed through this area (Figures 9c and 9d) and farther along the traverse (Figure 11a) are diagnostic characteristics of inflated lava (Self et al., 1998). We suspect that this is a primary P-type (Walker, 1989; Wilmoth & Walker, 1993) pahoehoe lava lobe preserved by burial in the section and excavated from the substrate during the emplacement of the ejecta.

Two examples of the lithomorphology are noted at the sol 122 and 124 locations. An upright angular fin-shaped rock avoided during the Sol 122 autonav drive (Figure 8c) bears sheeted tabular vesicle zonation, including a darker and finely vesicular possible chill margin face typical of the upper vesicular zone common to many lava flows (Aubele et al., 1988; Cashman & Kauahikaua, 1997; Sahagian, 1985). These are frequently horizontally jointed along planes following horizontal planar sheets and zones of variable vesicularity. Larger blocks exposed along the escarpment with Séítah to the west are characterized by similar planar jointing and close-packed vesicles, resulting in a scoriaceous appearance typical of upper zones within lava flows (Figure 9d). Preserved apparent upper surfaces of the source rock for some of these vesicular-appearing dark lithomorphologies and pavement-like polygonally jointed bedrock exposures (*e.g.*, *target Naltsos*) are visible in the Navcam panorama from the sol 124 location (Figure 9e). Although polygonally jointed on the surface as the *Nataani member* rocks, instead of granular surfaces surrounded by concentric exfoliation, these exposures are dense rocks that are orthogonally jointed in three dimensions. Smaller and more densely vesicular rocks lay on the surface, a characteristic typical of the upper meter of lava in which the surface is undergoing erosion. Exposures are dark on local outcrops where a thin coating of bright dust is removed. This basaltic lithology has been correlated with exposures capping Artuby Ridge in drives following sol 169 and sampled at the sol 180 location, the *Rochette member*, and are hereafter identified as *Rochette member*. This is a tentative field correlation in the absence of elemental analyses along the traverse here and it remains possible that the basaltic rocks along this part of the traverse are not the same as the *Rochette member* of Artuby Ridge farther to the south and west. Alternatively, the scattered dark vesicular rocks could be an expression of a lower unit, the *Roubion member* (discussed below in Section 3.2.4).

Horgan, Rice, et al. (2022) make a good case, using RIMFAX and Mastcam-Z spectral results that the polygonally jointed outcrops in this region are better correlated with and similar to the *Roubion member* observed farther to the south. They suggest that there is a possible sediment or thick regolith between the proposed *Roubion* and *Rochette members* noted here. The view along-strike to the south shows what appears to be regolith covering the contact zone between these exposures and an overlying rocky regolith, and farther east, overlying what is interpreted here as a *Nataani member*. The proposed *Nataani* exposures are identified in more proximal images in the sol 355 return mid-drive panoramas. Farther east are outliers of the *Ch'al member* that are overlying *Nataani members* based on observations at the eastern edge of the traverse between sols 66–78. Similar local relationships continue south through the sol 128 location.

Structural Characteristics. Linear troughs and fractures, striking approximately parallel to the escarpment bordering Séítah, are present but poorly expressed due to the substantial amounts of regolith cover. The RIMFAX findings in the traverse southwest of Adzillii Crater are more revealing where a reflector is identified 6 m below the surface. A looping traverse during the first Autonav drive test in this vicinity provided an opportunity to reconstruct the dip ($\sim 10^\circ\text{E}$) of the dense reflector showing that at least the section appears to dip uniformly east near the escarpment. This agrees in general with the apparent eastward stratigraphically stacked sequence exposing older to younger units. The rocky regolith appears to occupy a zone between the Séítah escarpment bedrock

seen in the Sol 124 and polygonally jointed *Nataani member* exposures to the east in agreement with this implied eastward-dipping sequence.

3.2.3. Southern Traverse, East Séítah Margin, Sols 130–136 and 353–354

Summary Field Interpretation Southern Traverse, East Séítah Margin. The fragments of the vesicle zone typical of the upper sections of lava flows indicate relative preservation of an original basaltic surface. Preservation is possible in an otherwise weathered terrain when a basaltic surface is protected by burial and is subsequently exhumed. If that is the case, then it supports the hypothesis that the *Rochette member* exposures along this part of the traverse are emerging from beneath *Nataani member* bedrock during erosion of the escarpment, a prediction from the westward up-dip projection to the local surface of dense reflectors observed by RIMFAX (Hamran et al., 2020, 2022).

The decline and disappearance of *Nataani member* exposures south of the sol 131 location in this segment of the traverse (Figure 10) is unusual. Misidentification is possible due to the limited observations during this part of the traverse. For example, the identification of *Rochette members* from sol 131 southward relies on panoramic images and could be incorrect. Also, it remains possible that all basaltic rocks south of that location in this segment are *Ch'al member* outliers. If so, then either an erosional trough or a down-dropped fault line formed in *Nataani* pre-*Ch'al* could explain the sudden termination of both surface exposures of *Nataani* and the eastern escarpment *Rochette*. These alternatives remain open because this is an area with few detailed observations.

Overview of the Traverse Segment. The traverse in this segment moves southeasterly beyond the sol 129 location and continues on fine regolith and mixed regolith with a *Rochette member* basaltic exposure to the west along the escarpment and *Nataani member* exposures to the east. Southward along the traverse, *Ch'al member* outcrops lie 60 m to the east with substantially smaller zones of *Nataani member* between the two. Exposures of *Nataani members* between *Ch'al* and *Rochette* appear to terminate to the south between the sol 131 and 134 locations. Alternatively, it is also possible that the blocks along the escarpment between sol 130 and 134 are disturbed blocks of *Nataani members*. These observations were confirmed on the return drives during the sol 353 through 354 drives farther east.

GXM Sols 130 - 136; 353-354

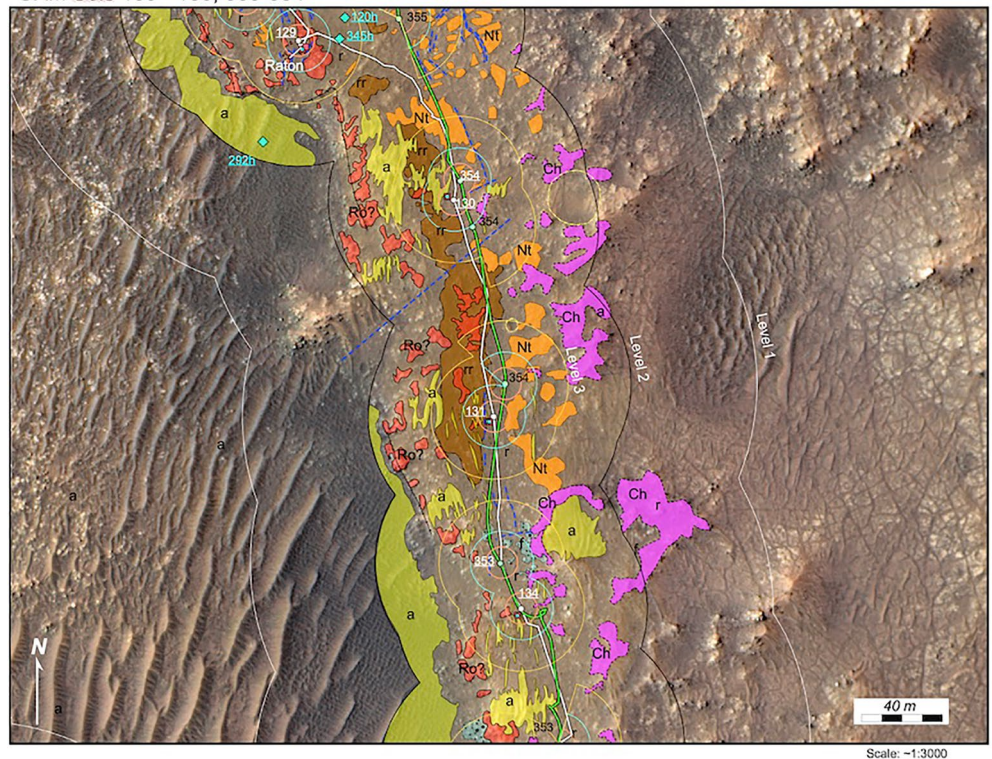


Figure 10. Geologic context mapping in situ geologic map traverse segment from sols 130–136; 353–354. Map units as in Figure 5 (White lines, inbound traverse; green lines, outbound traverse).

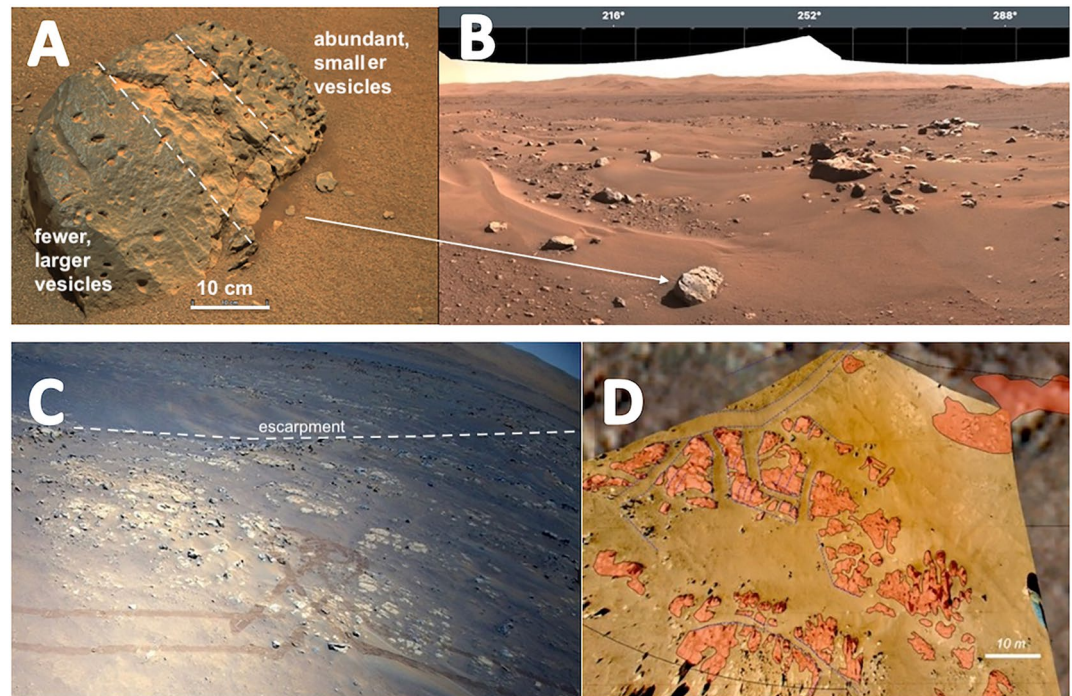


Figure 11. (a) Zcam image of vesicle zonation in Rochette float rock “*Castellane*.” The width of rock is ~50 cm. The vesicles range from 1 to 3 cm. Planar interface between “zones” of differing vesicle diameter as indicated is typical of the upper meter in inflated pahoehoe lava (type-P lavas) (ZRF_0135_0678921311_321FDR_N0050894ZCAM03179_0630LMJ01_Catellane). (b) View to the west from sol 124 location of mixed (“rocky,” map unit **rr**) regolith consisting of scattered Rochette float buried in regolith typical of the exposures near the Séítah-bounding escarpment from OEB landing site southward. The float rock *Castellane* is near the bottom center. Azimuths in degrees from sol 124 rover location indicated at the image top. N_LRGB_0134_RAS_0050894_CYP_R_SRERONVJ01 (c) Mapping on Ingenuity flight 9 image of *Rochette member* exposed along Artuby Ridge, sol 133 image directed west showing Rochette outcrops near the escarpment overlooking Séítah and rover tracks (2.1 m width) at the rover sol 124 locations. Orthogonally jointed outcrops characteristic of bedrock exposures of Rochette are also noted from surface views in Figure 5e (HSF_0133_0678747622_228FDR_N0090001HELI00000_000085J02; Balam, 2021). Mars 2020 Helicopter Camera Suite Bundle. NASA Planetary Data System (PDS). <https://doi.org/10.17189/1522845> (d) Orthogonally jointed bedrock outcrop habit is notable here as with examples on the east side of the Séítah escarpment in (c) Ingenuity image (sol 133 flight) 30–40 m south of the rover location on sol 341 location showing details of an exposure of the Rochette member (red) that are not visible in rover-based imaging (HSF_0133_0678747739_214FDR_N0090001HELI00007_000085J02; Balam, 2021). Mars 2020 Helicopter Camera Suite Bundle. NASA PDS. <https://doi.org/10.17189/1522845>.

Lithologies. Many of the characteristics of the dark rocks along the border with the Séítah terrain are indicators of basaltic lava flows. This includes the preservation of vesicle zones (e.g., the targets “*Castellane*,” Figure 11a) typical of the upper section of pahoehoe lava flows. The transition across the face of a basaltic block from low number densities of larger vesicles to smaller vesicles of high number density is common enough in the upper levels of pahoehoe lava that it is essentially diagnostic of inflated pahoehoe lava (Aubele et al., 1988; Cashman & Kauahikaua, 1997; Sahagian, 1985). However, the identification of basaltic lava exposures on the west side of the traverse as a *Rochette member* was not tested by contact measurements and is based largely on the assumption of continuity with basaltic exposures along most of the escarpment farther south. Considering that *Nataani member* exposures terminate after the Sol 130 position, and that we cannot trace the sequence of lithologies observed north of this location southward of the sol 131 position, alternative identification is that all exposures of basaltic rock southward are *Ch'al members* rather than *Rochette*.

Mixed regolith is more common along this part of the escarpment. Many of the blocks within the mixed regolith exposures are clearly locally derived *Rochette members* (Figure 11b), implying that mixed regolith in this region is at least a local *Rochette member* float acting as obstructions to Aeolian transport that traps and accumulates substantial mantles of aeolian material.

Structural Characteristics. On flight 9 (Sol 133), the *Ingenuity* helicopter ascended near the *Perseverance* sol 129 location, crossed the escarpment, and flew to the Artuby Ridge. Both the ascent site and landing sites occurred over *Rochette member* outcrops providing an areal view in the high-resolution color camera data of the orthogonal jointing typical of *Rochette* outcrops (Figures 11c and 11d). The relatively orthogonal pattern of joints on flat-lying texturally rough and pitted surfaces are typical of basaltic lavas where erosion has removed the upper few tens of centimeters upper vesicular zones consisting of centimeter to decimeter joint blocks and cobbles (Aubele et al., 1988). The preservation of the morphological details in the upper meter of a flow that has been covered by later material units is consistent with the interpreted exhumation of the *Rochette member* from a *Nataani member* cover along this part of the traverse.

3.2.4. Mure-Artuby (South Séítah Margin) (Sols 135–171; 351)

Summary Field Interpretation of the Mure-Artuby (south Séítah Margin). This is a complex area to interpret as there are several observations that question the initial interpretation that this area represents a *Rochette member* capping another *Nataani*-like lithology, the *Roubion member*. Farther along this segment of the traverse the appearance of yet another lithology, the *Artuby member* (Figure 12), between the *Roubion* and *Rochette members* at *Mure* adds more complexity to tracing contacts. The interpretation of the *Artuby member* is also complicated by relatively few observations between the initial exposures seen at *Mure* and its apparent continuation along Artuby Ridge to the west. The presence of dense upper vesicular zones within the eastern escarpment segment and dense, ellipsoidal interior structures and basal foliations at *Mure* support the interpretation of *Rochette member* as a basalt flow preserving upper, interior, and basal structures typical of P-type (Wilmoth & Walker, 1993) basaltic lavas.

Bench-like steps several centimeters in relief are potentially expressions of the layered or foliated structure typical of the *Artuby member* along the slope from the *Rochette* outcrop to the *Roubion member* polygon area. Dark protuberances on the upper surface of *Roubion member* polygons are similar to those seen in the *Nataani member* of proximity to *Ch'al member* outcrops. Here, it can be argued that these dark protuberances are the more coherent

GXM Sols 135 - 171; 351

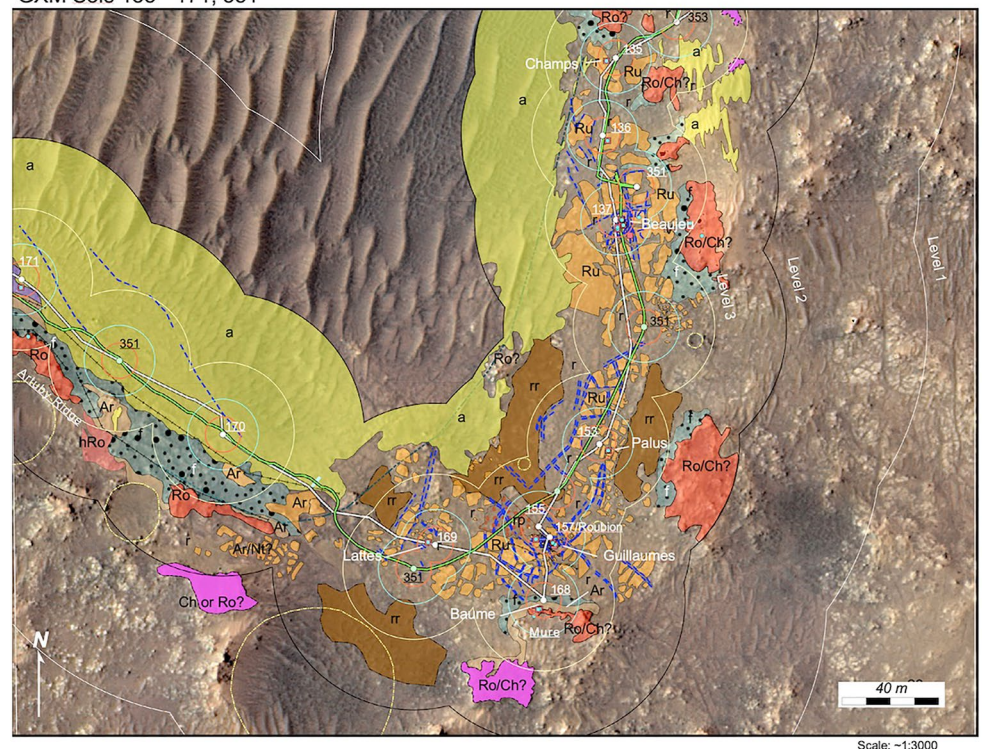


Figure 12. Geologic context mapping in situ geologic map traverses a segment from sols 135–171, 351. Map units as in Figure 5 (White lines, inbound traverse; green lines, outbound traverse).

ent interiors of *Artuby member* interior “layer” segments seen farther west along the slopes of Artuby Ridge. This would suggest that the *Artuby member* grades downward into *Roubion* and is an upper facies of the *Roubion* lithology.

Overview of the Traverse Segment. The traverse continues southward for approximately 200 m dropping in elevation through a small pass to lower benches of polygonally jointed outcrops abutted on the east by resistant cap rocks of dark, massive boulders consistent with mafic compositions (Figure 13a). The traverse continues following the margin with Séítah where it bends to the northwest at Mure and follows the Artuby Ridge offering several opportunities to observe sectioned views of the lithologies. The drive from the southernmost point of the bend in the traverse toward the lower slopes of Artuby Ridge between sols 169 to sol 170, and subsequently the return rapid traverse on sol 351, did not acquire sufficient image data to confirm the stratigraphic relationship and contact between the *Roubion member* and *Artuby member* beyond the sol 170 location. Either the *Roubion member* thins westward or is unexposed beneath the slopes of Artuby Ridge. Alternately, there are centimeter-scale steps or benches between the sol 155 location where Perseverance was situated on typical *Roubion member* bedrock (Figure 13b) and the obvious foliated *Artuby member* exposures beneath the apparent *Rochette* cap rock to the east. The benches could be an oblique section through the lower portions of the *Artuby member*, which is distinguished farther along the traverse by thicker centimeter-scale layers or foliations. If the *Artuby member* is exposed in surface exposures between the sols 168 and 170 locations as small benches in the terrain instead of sectional views as elsewhere, it could resolve some of the ambiguity in the contact between Artuby and Roubion members farther west. In this case, then *Roubion member* is not visible farther west because it lies beneath the *Artuby member* along the slopes of Artuby Ridge where thick regolith and aeolian bedforms present the bedrock of the slope.

Collectively, the observations along this segment might imply that the section is *Nataani member* capped by *Ch'al member*, a field interpretation that is difficult to reconcile unless the dark cap rocks are not a southward continuation of the escarpment bounding *Rochette member* noted up to this point in the traverse. Either this area represents a repetition of the section through an otherwise undetected fault dropping the section in elevation, or erosion of a valley, removing *Rochette* in the vicinity and prior to the emplacement of *Nataani* and *Ch'al* (Horgan, Rice, et al., 2022). The latter would imply that the dark and vesicular surface of the bench near sol 137 is the upper surface of *Roubion* as detected farther south, that the dark cap rocks to the east at this location are *Ch'al*, and that *Nataani* lies between the two units. This is supported somewhat by RIMFAX data and local spectral data (Horgan, Rice, et al., 2022). In general, the transition in lithologies and observable stratigraphic relationships is confusing in this segment of the traverse and subject to debate and future revisions.

Lithologies. Between sols 135 and 159, the traverse proceeds over the surfaces of polygonally jointed granular outcrops of *Roubion members*. Physical characteristics of the *Roubion* lithology in images over this area are essentially identical to *Nataani member*. This includes the prevalence of dark protuberances in the upper surface of *Roubion* polygons particularly in the slope immediately below the dark mafic rocks to the east, much like the dark protuberances on *Nataani member* exposures in proximity to the mafic rocks of the *Ch'al member*. At the sol 137 location, extensive pitting within the dark protuberances with characteristics of vesicles and in places appearing moderately scoriaceous, also echo the physical characteristics of the dark protuberances observed in the *Nataani member* (Figures 13a and 13b). The contact with the dark mafic boulders capping the escarpment 70 m to the east along this section is, similar to the *Nataani-Ch'al* contact, obscured by scree and float spalling from the more resistant cap rock (Figure 13c).

Rochette member exposures were observed in proximity at the sol 168 location. These are dark, massive exposures bearing vesicle sheets and ellipsoidal masses typical of the basal interior of lava flows (Self et al., 1998) (Figures 13d and 13e). Together with the prevalence of vesicular texture observed in *Rochette* exposures throughout the traverse of the interior structure is evidence that these are lava flows here exposed in section. Both vesicular zonation and interior ellipsoidal structures are almost uniquely characteristic of inflated lava flows (Walker, 1991). This represents the first clear example of lava flow cross sections seen on a surface mission on Mars and expands our understanding of basaltic lava flow morphology and structure from their surfaces to the interiors.

Finely foliated and somewhat granular materials are exposed beneath this section (Figure 13e) typical of a zone that continues westward beneath capping *Rochette member* outcrops along Artuby Ridge.

Structural Characteristics. Surface structural features in the *Roubion-Mure* area are similar to those observed along the traverse north of this location: linear trough-like fractures several tens of centimeter wide and approx-

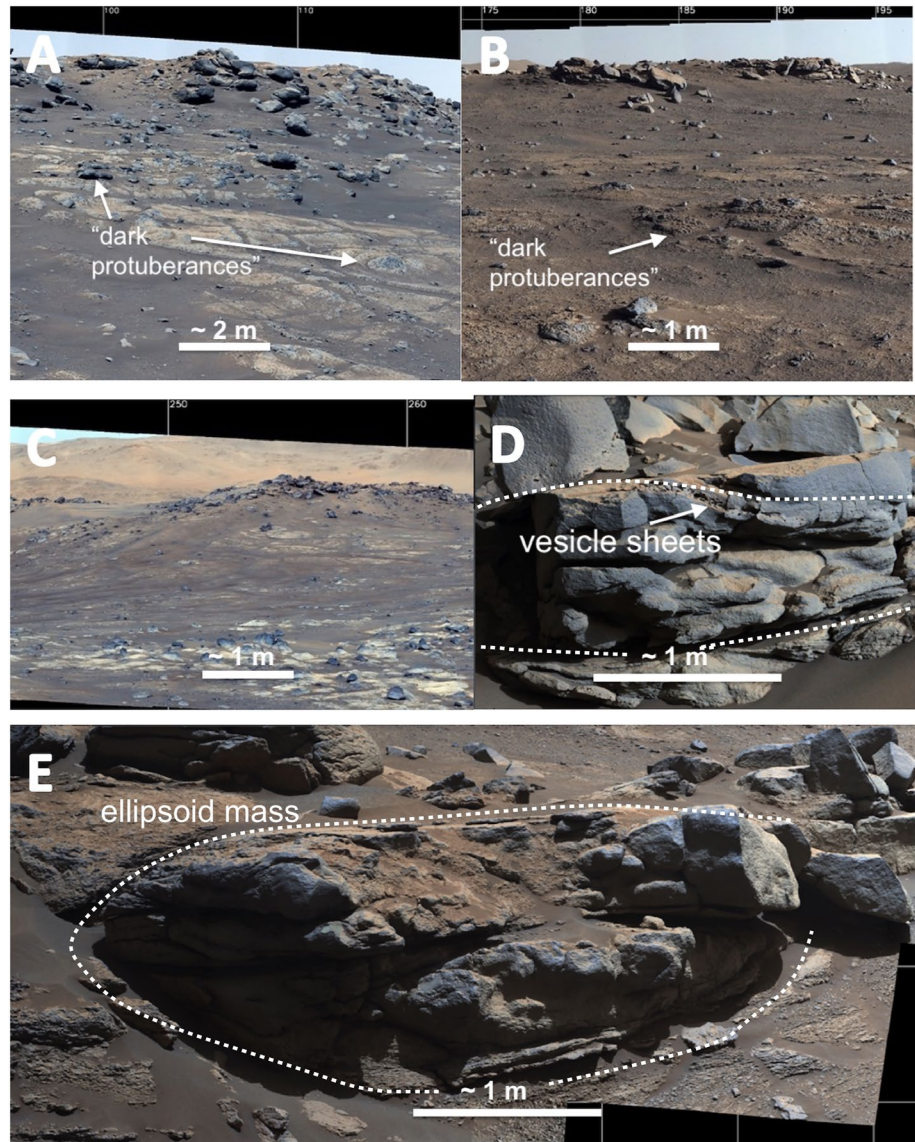


Figure 13. (a) East-directed section view of escarpment at sol 137 location showing polygonally jointed granular outcrops of *Roubion member* with dark vesicular protuberances near contact with overlying *Rochette member* or what may also be broken sections of *Nataani member*. Image QZCAM_SOL138_139_ZCAM08147_8148_L0_Z110_CFFR_TRANSITION_4X_E01. (b) View south from the sol 155 location near the *Roubion member* sample attempts showing regolith covered *Roubion member* with dark vesicular protuberances. Image QZCAM_SOL0155_ZCAM07000_L0_Z110_DRIVE_DIR_PDI_E01. The covered contact with *Rochette* and *Artuby member* exposures caps the local escarpment in the distance at *Mure*. The transition may be compared with the *Nataani-Chal* transition (Figure 2a). (c) Southwestward-directed view from sol 170 location at the east end of *Artuby Ridge*. Image QZCAM_SOL0170_ZCAM08183_R0_Z110. *Rochette member* overlies horizontally foliated exposures of *Artuby member* with *Roubion member* in the foreground populated by dark protuberances. The *Artuby member* either pinches out eastward or is unexposed in image (a) from sol 137 location. The *Roubion member* is not observed westward of the sol 170 location in (c). (d) Outcrop of *Rochette member* at *Mure*. Image QZCAM_SOL0168_0169_ZCAM08180_ZCAM08181_L0_Z110_MURE_PDI_NEAR_OUTCROPS_E02. Curvilinear sub-horizontal vesicle sheets and ellipsoidal masses (enclosed with dashed line) are similar to structures typical of basal interior late-stage flow in lava flows (e.g., Self et al., 1998). (e) Contact between *Rochette* ellipsoidal basal structure (enclosed with dashed line) and finely foliated character of *Artuby member*. The similarity of this view with *Artuby* seen farther along *Artuby Ridge* suggests that the *Rochette member* may also grade downward into the *Artuby member*. Image QZCAM_SOL0168_0169_ZCAM08180_ZCAM08181_L0_Z110_MURE. Similar fine foliations at the contact with *Rochette* are observed elsewhere on *Artuby Ridge* encountered in subsequent sols (d and e) Are segments of image QZCAM_SOL0168_0169_ZCAM08180_ZCAM08181_L0.

imately parallel to the escarpment and contact with Séítah. This continues in scale down to meter scales. Within individual polygons, fractures are more irregular in orientation and length and separated by centimeters. Fracturing is not limited to regional structures but includes individual outcrops. At the sampled polygon “Roubion” and the abrasion target “Gaulleumes,” irregular fractures are pervasive to centimeter scale.

3.2.5. Artuby Ridge (South Séítah Margin) (Sols 171–200; 340–343)

Summary Field Interpretation of Artuby Ridge (Sols 171–200; 340–343). This segment of the traverse (Figure 14) provided an opportunity to view a section of the escarpment bounding Séítah to the north, where the apparent dips are oriented south-southeast. Exposures along the face of the Artuby Ridge provide a view of the sequence from grussy, foliated *Artuby member* contacts to the overlying resistant caprock of the *Rochette member* atop the Artuby Ridge. Fractures trending at right angles and those trending parallel to the escarpment edge could represent a response to strain associated with the development of the escarpment. Alternately these could have developed during uplift and tilting of the sections associated with the creation of the relatively high terrain of the stratigraphically lower *Séítah formation* rocks through some poorly understood process of regional uplift centered on the Séítah terrain (Farley et al., 2022).

In this case, the fractures may be simple scissors faults, as some of the outcrop mapping implies.

Overview of the Traverse Segment. Artuby Ridge follows the contact between older lithologies of Séítah to the north and the resistant igneous lithologies of the *Máaz formation* to the south. *Perseverance* transitions to a west-northwest drive direction following the strike of Artuby Ridge until sol 178, where the traverse moves onto the caprock. The purpose of the traverse is to examine the stratigraphy and structure of a potentially exposed section of the lower *Máaz formation* with a bench 20–30 m wide sloping to the north-northeast from the escarpment that provides an easily traversed route from which the inspection of exposures is possible. On the east half of the Artuby Ridge, the terrain slopes gently down to a contact with *Séítah formation* locally covered along most of the slope by aeolian bedforms. One of the more notable exposures of the Artuby member lithology within the

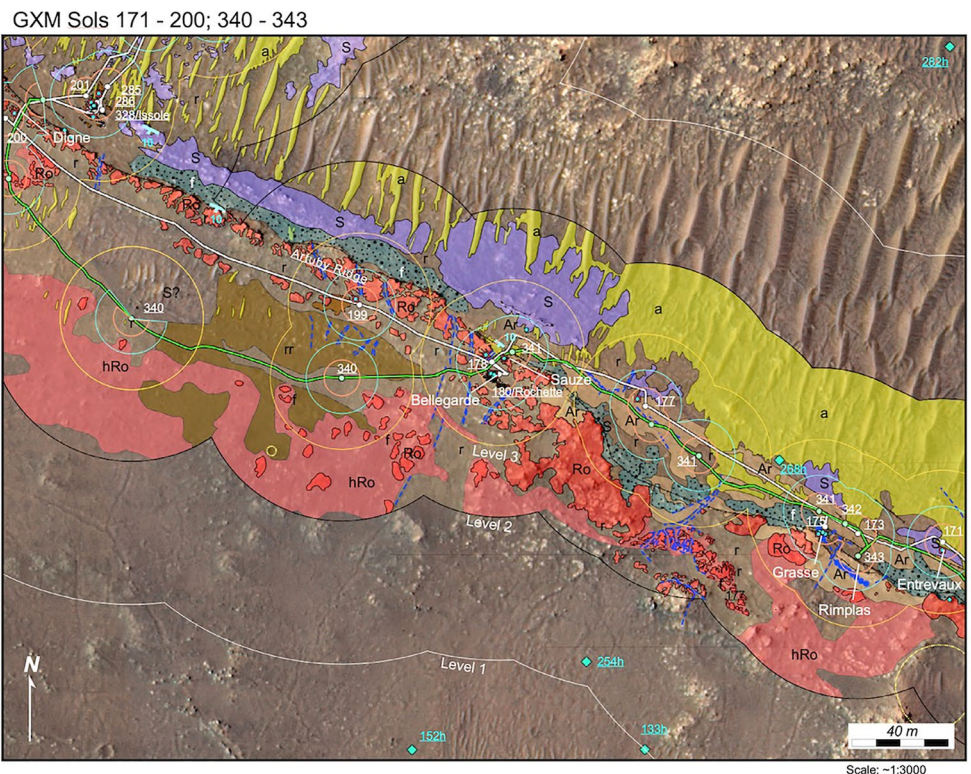


Figure 14. Geologic context mapping in situ geologic maps traverse segments from sols 171–200 and 340–343. Map units as in Figure 5 (White lines, inbound traverse; green lines, outbound traverse).

escarpment (“*Rimplas*”) occurs along the lower slopes here. The “*Rimplas*” outcrop was examined during the return traverse.

On Sol 178 *Perseverance* ascended the Artuby Ridge at “*Citadelle*,” where the contact between the overlying Rochette member and the *Artuby member* is well exposed, for sampling of the resistant caprock at the target “*Rochette*.”

Lithologies. Artuby member exposures along the upper slopes of Artuby Ridge are covered by a float along most of the length but are well exposed in several locations. The upper and lower visible sections of the *Artuby member* appear to be divided into recessive and more resistant zones (Figure 15a). In contrast to finely foliated sections noted at Mure (Sol 168) and elsewhere immediately beneath the *Rochette member* cap rock, in the eroded face of Artuby Ridge along the eastern third of Artuby Ridge an approximately 30 m horizontal outcrop at “*Rimplas*” (Sols 340 to 343) (Figures 15b and 15c) shows a transition downward from the recessive behavior of the upper finely foliated part of the *Artuby member* noted at *Mure* (Sol 168) to the more coherent, layered characteristic of the lower section. The recessive character has resulted in southeasterly retreat of the Rochette member caprock escarpment approximately 10 m south from its location on the northwest and southeast at this location (Figure 15c).

Exposures along the lower sloping surface along the traverse path are few as the slope is largely covered with aeolian bedforms and thick fine regolith. A couple of exposures along the slope (near the sol 171 location, “*Entrevaux*,” are determined to have LIBS spectra consistent with the presence of olivine (Wiens et al., 2022), a characteristic of the *Séítah formation*. This observation implies that the contact between *Mááz formation* and *Séítah formation* may lie within the lower slopes of Artuby Ridge. Elsewhere along the lower slopes, the regolith

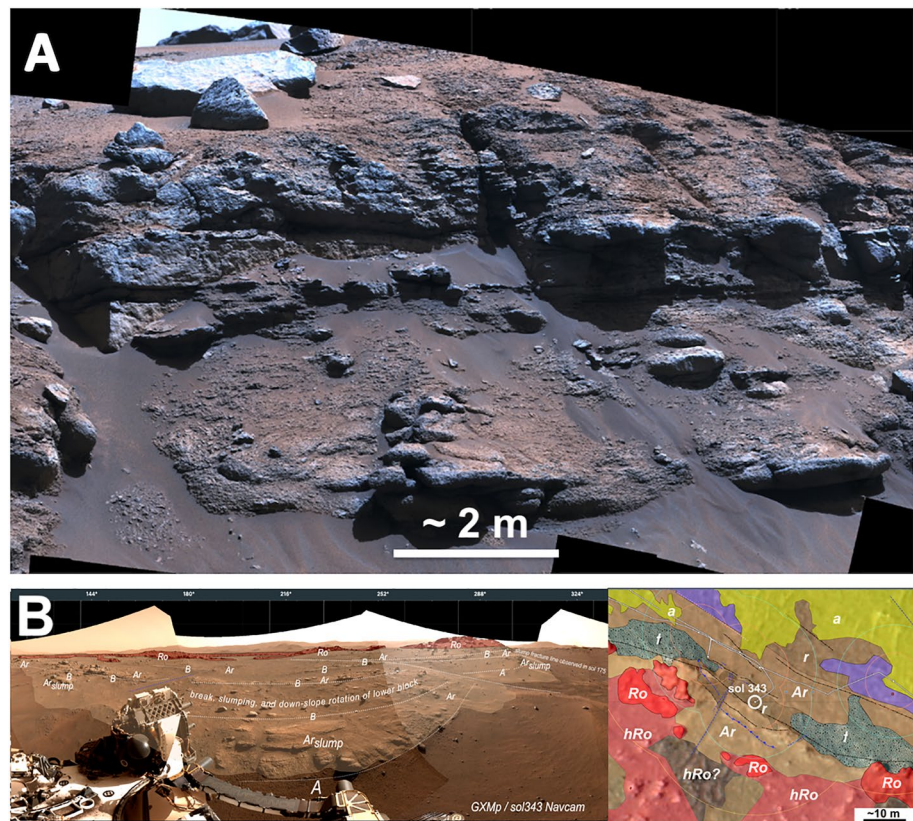


Figure 15. (a) Lower section of the Artuby member at the sol 175 location of the Séítah-facing Artuby Ridge escarpment showing slabs, concentric shell-like weathering around coherent rock exposures, and grussy intervening zones typical of the *Artuby member*. Image QZCAM_SOL0177_ZCAM08190_L0_Z110_ARTUBY_VAUCLOSE_AURIBEAU_E0B. (b) Geologic context mapping (GXM) perspective geologic map of “*Rimplas*,” an *Artuby member* outcrop characterized by thick layers and foliations exposed in the lower face of Artuby Ridge. Image N_LRGB_0343_RAS_0092982_CYL_S_AUTOGENJ01 C. Expanded view of GXM map details in the vicinity of “*Rimplas*.”

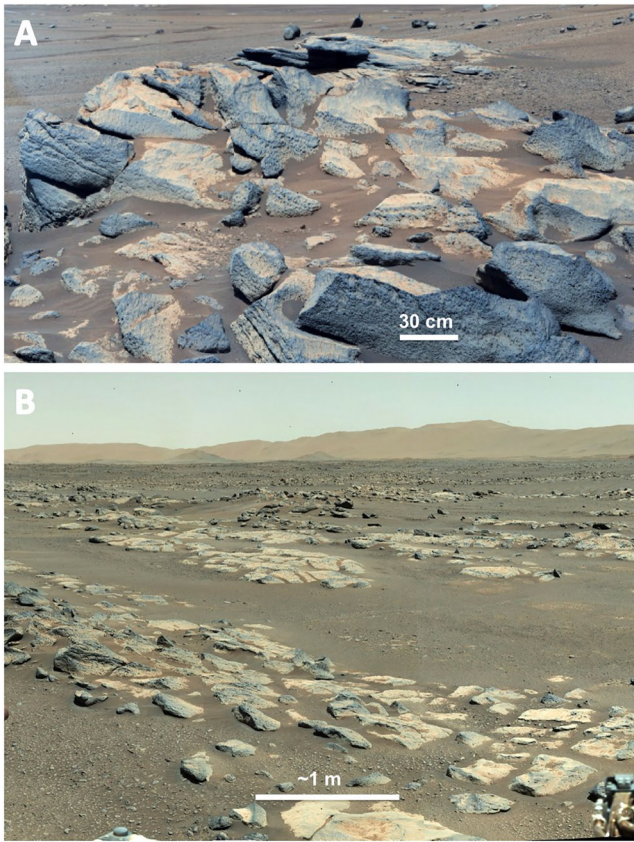


Figure 16. (a) View southeast along the crest of the Artuby ridge of foliations and vesicle sheets in the vesicular Rochette member cap rock outcrop dipping south-southwest at approximately 8°. Image QZCAM_SOL0180_ZCAM08196_R0_Z110_ENTRAGES_CITADELLE_E01. (b) South-directed view across sub-polygonal, orthogonally jointed blocks that characterize the surface of the Rochette member atop Artuby Ridge. This image was acquired near the Rochette core and sample site. Image QZCAM_SOL0181_ZCAM08199_L0_Z034_180_DEG_MOSAIC_SOUTH_E01.

is patterned with vague polygonal patterns that may be the expression of a polygonally jointed surface immediately beneath the regolith cover. These may be indicators of the unexposed continuation of the *Roubion member* westward from the last exposures observed near Mure.

Ascent onto the Artuby Ridge caprock beginning on Sol 178 (“Citadelle”) provided an overhead view of the *Rochette member* upper surface (Figures 16a and 16b). The exposures of the *Rochette member* occur as sub-polygonal, somewhat prismatic, and vesicular blocks arrayed on a regolith dominated low-relief surface continuing southeastward from the escarpment edge. The transition between Rochette caprocks and Artuby observed during the ascent onto Artuby Ridge on Sol 178 is characterized by a basal slabby and fissile style within the lower exposures of the Rochette member, grading rapidly to the more finely foliated and “grussy” upper part of the Artuby member noted above.

Southward the *Rochette member* outcrops appear scattered with intervening regolith or exposures of the underlying *Artuby member* and are mapped as “hummocky Rochette unit (hRo). Again, a vague pattern of fractures within the areas between hummocks is potentially related to exposures of the more complexly fractured underlying *Aruby member*.

Structural Characteristics. All exposures in the escarpment dip south-southeast along the face of Artuby Ridge. Along-strike viewing to the east during the ascent on sol 178 and from the sol 200 location at the western end of Artuby Ridge have approximately 10° apparent dips to the south-southwest within 60 m of the escarpment. This is confirmed in the sub-surface by RIMFAX sounding along traverses that occur on traverses at right angles to the strike of the escarpment.

On the upper surface of Artuby Ridge and within the *Rochette member*, the larger trough-like fractures that characterize much of the surface throughout the *Máz formation* are generally oriented at right angles to the strike of the escarpment (Figure 14). This contrasts with the escarpment-parallel trend observed east and north along the traverse. A northeasterly oriented fault in the outcrop at the site “*Rimplas*,” sol 343) appears to displace the visited section downward to the north relative to the surrounding escarpment sections. Similar faults elsewhere along the escarpment (e.g., sol 175 section), all of which die out to the south, are interpreted as simple scissors faults that would be consistent with uneven uplift of the section along a zone of deformation around Séítah.

A minor subset of fracture trending parallel to the escarpment occurs within exposed areas of the *Rochette member* and defines prismatic blocks. An example is the Rochette type lithology that was cored and sampled at the Sol 180–198 location.

3.2.6. Séítah (Sols 199–340)

Summary Field Interpretation of Séítah (Sols 199–340). The traverse entered Séítah following descent from Artuby Ridge on sol 201 (Figure 17). One model of the stratigraphy prior to the traverse into Séítah proposed that *Séítah formation* was an exposure of the fluvial sediments presumably pre-dating most of the crater floor units and that olivine, identified from orbital remote sensing (Horgan et al., 2020) would be more abundant. Although the modal abundance of olivine was unresolvable with the abraded exposures examined, olivine was detected via in situ analysis in Séítah exposures as predicted. However, exposures visited at *Bastide* on the lower slopes of a Séítah hill and the overlying *Caille* exposures do not identify any unequivocally sedimentary materials. Instead, a collection of potential mafic rocks bearing planar fissile behavior and petrographic cumulate textures (Liu et al., 2022; Schmidt et al., 2022) are observed, similar to those in many thick terrestrial mafic sections (Jerram et al., 2003).

Seitah traverse/ Sols 199 - 340

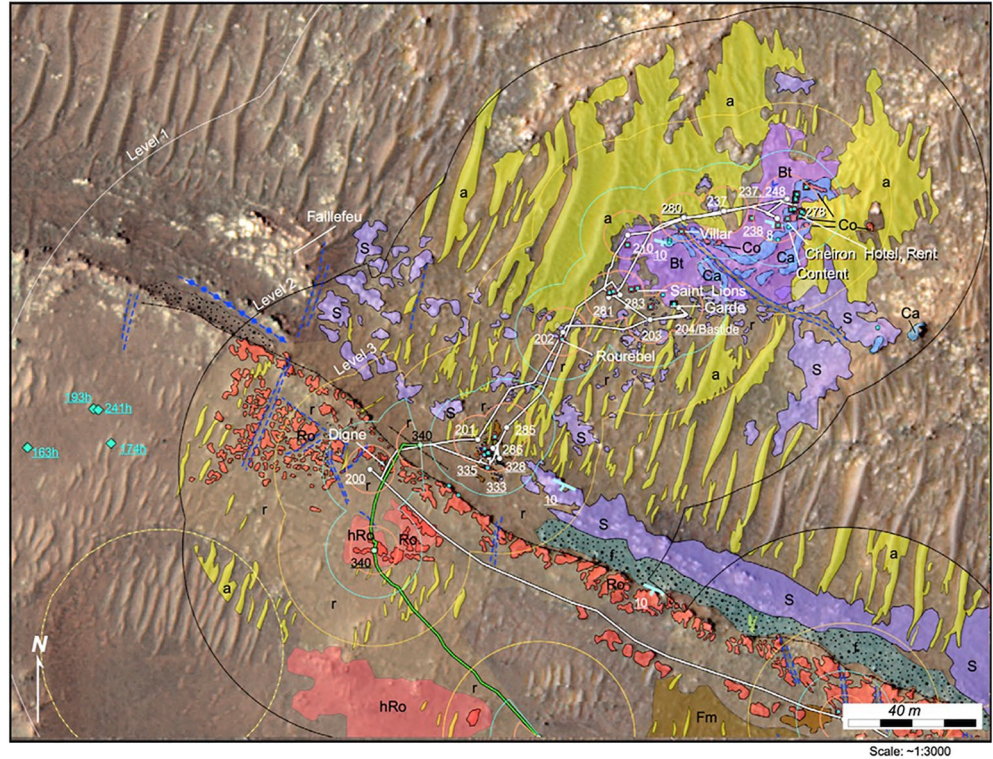


Figure 17. Geologic context mapping in situ geologic map traverses a segment from sols 199–340 (White lines, inboard traverse; green lines, outbound traverse).

A general characteristic of exposures along Artuby Ridge is the persistent south-southwesterly dips of contacts, layers, and foliations. This south-southwesterly dip is shared with all the exposures along the traverse into Séitah.

Other lithologies, notably along the contact with *Máaz formation* near Artuby Ridge (*Issole* outcrop) are granular, somewhat friable lenses of a material that appears to be substantially altered. Neither clear igneous nor sedimentary textures are discernible for these exposures and the emplacement mechanism remains undetermined.

Because of the presence of vesicles up to a few millimeters in diameter in *Content*, it is interpreted to be the remains of either a lava flow or the upper section of a thick magma body at or near the surface at the time of emplacement. *Content* appears unrelated to the underlying Séitah lithologies because a diagnostic characteristic of Séitah rocks, the occurrence of detectable amounts of olivine, is unobserved in the *Content* examples examined. This relative absence of olivine relative to Séitah rocks supports an interpretation that *Content* likely represents a different, unrelated phase of igneous activity.

Projecting up-dip from Séitah formation outcrops at *Issole* near the basal contact with the *Máaz formation* implies that *Issole* and many of the scattered exposures are stratigraphically above the *Bastide* member and possibly above the *Caille* and *Brac* members. If so, the apparent advanced alteration of the exposures at *Issole* compared to those within *Bastide*, *Caille*, and *Brac* could result from the part of the section closest to the surface, *Issole*, experiencing deeper weathering than *Bastide*, *Caille*, and *Brac* units because they were somewhat deeper in the section.

The Séitah formation is complex both in terrain characteristics and lithology, challenging models for its emplacement and relationship, if any, to the overlying *Máaz formation*. The identification of potential cumulate textures in *Brac* implies an intrusive or thick extrusive origin (Liu et al., 2022; Schmidt et al., 2022).

Overview of the Traverse Segment. Examination and sampling of the oldest geologic unit accessible, Séitah, was an important objective of the crater floor campaign. The traverse proceeds from Artuby Ridge beginning on Sol 201 northeast across the lower slopes of Artuby Ridge and across a broad moat-like depression at the boundary

between Séítah and Artuby Ridge in order to visit exposures in a hill (Caille) typical of the chaotically arrayed relief within Séítah as a whole. The return traverse to Artuby Ridge crosses the intervening scattered exposures and completes the stratigraphic and in situ observations between Sol 286–339 at the outcrop “*Issole*” located near the upper contact with *Máaz formation* at the base of Artuby Ridge.

Lithologies. Field observable lithologic characteristics of *Séítah formation* exposures are characterized by massive fine-grained to granular and resistant layers and foliations, frequently disintegrating into slabby and tabular floats paving the slopes of Séítah hills. Three distinct members with these characteristics identified include “*Bastide*,” “*Caille*,” and “*Brac*” (Figures 18a and 18b). A fifth lithology (*Séítah, undivided member*, unit **S**) is the site of sampling and is exposed at the outcrop “*Issole*” where samples were acquired on tabular, south-southwesterly dipping outcrops of coarse grained, slightly lineated materials characteristic of the exposures near the contact with the slopes of Artuby Ridge (Figure 18c).

A fourth identified lithology, “*Content*,” is anomalous in comparison with *Bastide*, *Caille*, and *Brac*. While *Bastide*, *Caille*, and *Brac* are dense, fine-grained rocks with no macroscopic texture except planar sheeting, *Content* consists of disaggregated clusterings of sub-rounded scoriaceous-appearing materials resting at the top of the visited Séítah hill. Vesicles up to several millimeters in diameter are a principal characteristic of *Content* rocks. *Content* lithology does not contain identifiable olivine in Supercam results (Wiens et al., 2022), unlike

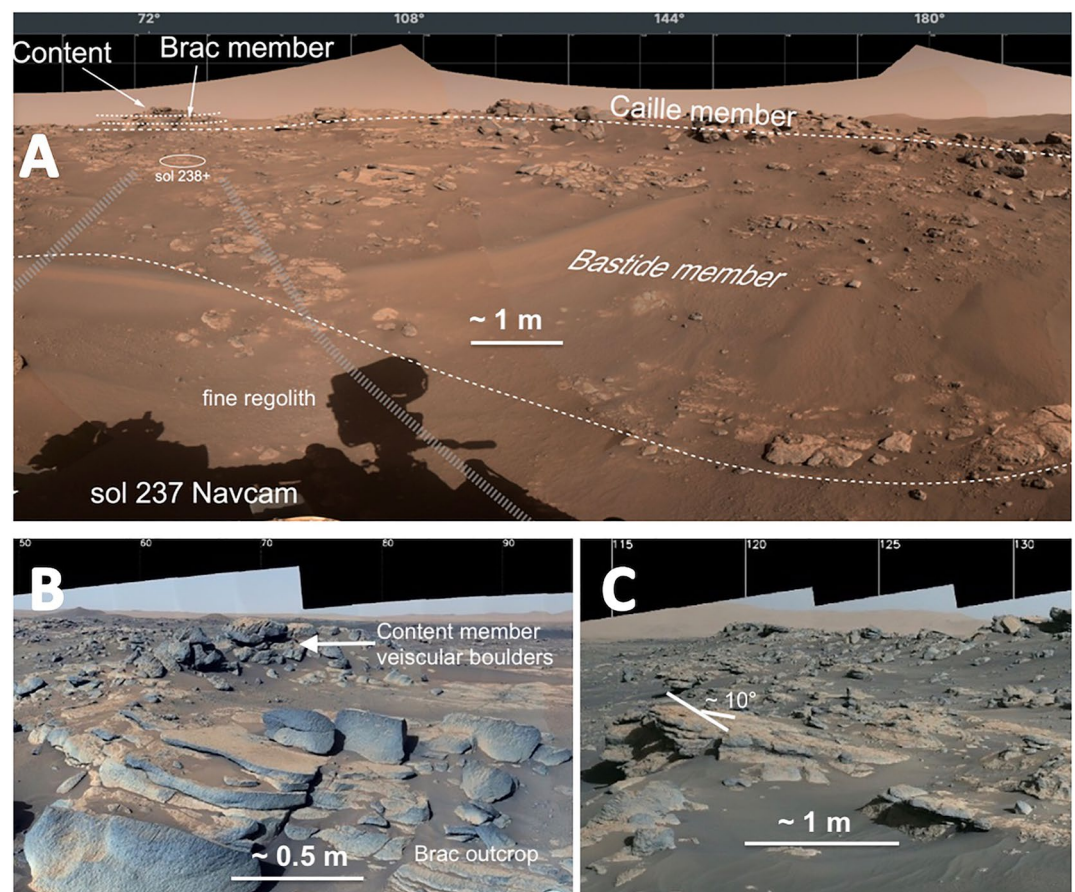


Figure 18. (a) Arrangement of *Bastide*, *Caille*, *Brac*, and *Content* member exposures in Séítah hill. Part of Navcam panorama N_LRGB_0237_RAS_0072246_CYL_L_AUTOGENJ03 (b) *Brac* outcrop, site of sampling (Simon, Amundsen, et al., 2022; Simon, Hickman-Lewis, et al., 2023), overlain by clustered vesicular boulders of *Content* member capping the ridge in the distance. QZCAM_SOL0240_0241_ZCAM08264_ZCAM08266_L0_Z110_CAILLE_LAYER_TRANSITION_DANI_DIT_ITI_DISTANT_OUTCROP_E01 (c) Along-strike viewing of the continuation to the southeast of the *Issole* outcrop (*Séítah, undivided member*), dipping approximately 10° to the south-southwest near the contact with *Máaz formation* on the lower slope of Artuby Ridge. *Rochette member* underlain by local *Artuby member* exposures cap Artuby Ridge on the upper horizon. QZCAM_SOL0289_ZCAM08314_L0_Z110_ARTUBY_RIDGE_EXT_E01.

the other Séítah rocks examined. In this respect, and because of the presence of what are interpreted as vesicles, *Content* is more comparable to rocks typical of the *Máaz formation*, particularly *Rochette member* rocks.

Structural Characteristics. Foliations and layers throughout the traverse across the *Séítah formation* appear to dip approximately conformably with the southwest dips noted along Artuby Ridge in the *Máaz formation*, a characteristic confirmed by RIMFAX observations (Hamran et al., 2022). Dips atop the Séítah hill are a few degrees lower than those to the south.

A few fractures occur within the *Séítah formation* similar to the *Máaz formation*. Instead, the identified fractures are more arcuate and snake across the hills at overall strikes to the northwest. One example approximately 1 m wide crosses the visited Séítah hill where it displaces exposures of the *Bastide* and *Calle members*. Analysis of the geometries of dips in outcrops along the crest of the Séítah hill relative to dips south of the fracture shows lower angle dip north of the fracture, potentially resulting from simple mode 1 crack behavior that has rotated the section northward across the fracture (Tate et al., 2022).

Representative clusters of *Content member* boulders rest unconformably across the surface of the underlying *Séítah formation*, either as resistant residuals displaced during the erosion of the Séítah hills, or by initial emplacement on an eroded surface. Observations are insufficient to identify which scenario is more likely.

4. Summary Interpretation, Main Results, and Discussion of Geologic Context Mapping

Séítah was identified as an older terrain (*Séítah formation*) in which olivine was present and overlapped by younger crater-retaining terrains (*Máaz formation*) in pre-landing remote sensing and photogeologic mapping (Sun & Stack, 2020; Stack et al., 2020). *Perseverance* traversed along the southern contact between these two Jezero Crater floor geologic units, observing the elemental, mineralogical, and petrographic character of the lithologies of both formations and confirming the presence of olivine in Séítah determined from orbital remote sensing (Brown et al., 2020; Horgan et al., 2020).

Prior to the *Perseverance* traverse, however, deposits of sediments or regional ash falls remained a possible explanation of many of the observed sheeted and overlapping floor units (Farley et al., 2022; Stack et al., 2020; Sun & Stack, 2020). In situ mapping of the lithologies on the crater floor along the traverse at a scale of approximately 1:3000 instead identifies a complex collection of lava flows, deeply altered more massive basaltic rocks and olivine-bearing holocrystalline rocks that may be intrusive. The erosion and alteration together with the limited reconnaissance style of the mapping and difficulty in interpreting possible protoliths for many of the exposures complicate the confident interpretation of the stratigraphic relationships and structure of the crater floor. Our results, particularly regarding stratigraphy, must remain a “best fit” to the observations. Nonetheless, some fundamental field relations can be identified.

Examples of aerial mapping using *Ingenuity* as a reconnaissance geologic platform (Figures 6f, 10c, and 10d) illustrate the potential utility of aerial platforms as a means of extending in situ mapping knowledge beyond the rover perspective. In situ style geologic mapping on helicopter-based mosaics and single frames (Figure 10d) has also shown that aerial images may be used much like air photos in the field on Earth to plan and test mapping hypotheses prior to the actual surface examination or to extend mapping and known contact relationships into areas unvisited by rovers.

4.1. General Results

To aid the visualization of the general findings from in situ mapping, an interpretive bedrock map is provided in Figure 19a that connects the scattered exposures of units and interpolates between outcrops. While this presents a gross simplification of the mapping results, it outlines the principal areas over which the identified lithologies occur and more clearly illustrates the correlation with larger pre-landing photogeologic mapping units.

The *Máaz formation* of in situ mapping correlates well with the “crater floor, fractured, rough” unit (*Cf-fr*) as mapped in Stack et al. (2020) with an allowance for minor differences in the location of contacts appropriate for the differences in mapping scales. The “crater floor fractured” unit (*Cf-f-I*) likewise agrees with the mapped *Séítah formation*, while the “undifferentiated smooth” unit (*Us*) captures the broader areas covered with substantial regolith identified in the in situ mapping.

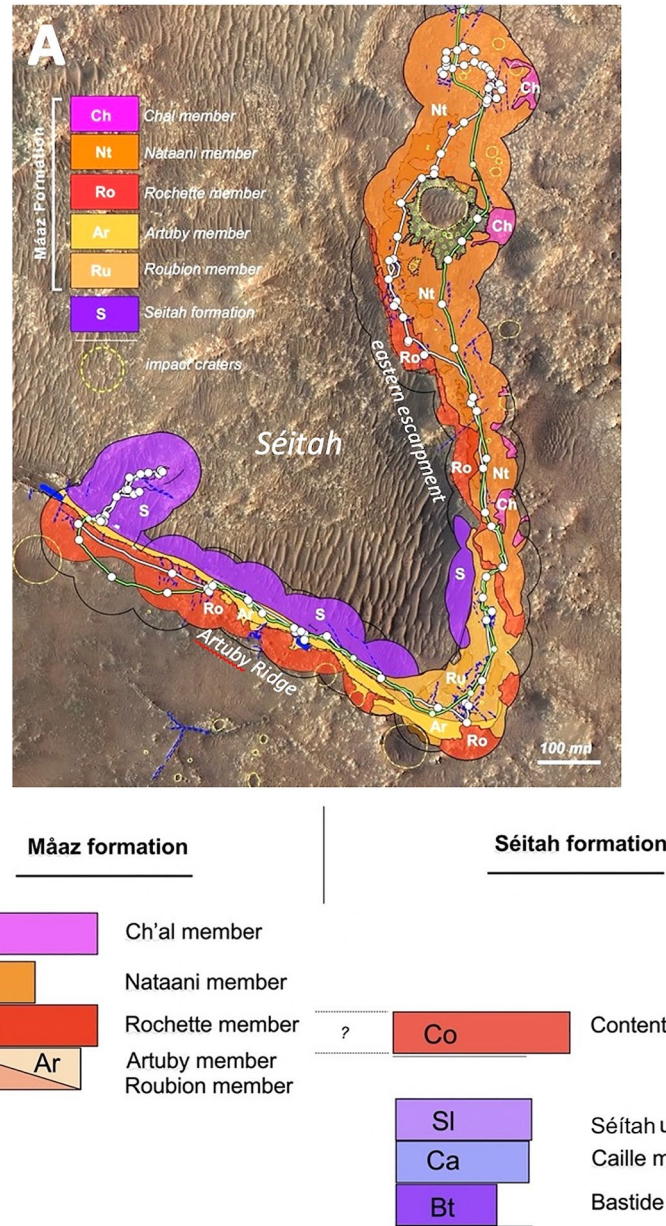


Figure 19. (a) Summary interpolation of the extent of bedrock geologic units based on in situ mapping. The width of the mapping corridor is ~120 m (Level 2). White dots are positions occupied during the traverse for which images are available for mapping. (b) Summary of interpreted stratigraphic relationships between identified lithologic units along the Jezero Crater floor traverse.

Apart from morphologically fresher craters (assumed to be younger) such as the Adziillii crater and a few meter-scale craters located in the regolith, most impact craters in the bedrock along the traverse and on the crater floor in general are severely eroded and are little more than circular depressions within the regolith. Erosion across the youngest unit (*Ch'al member* lavas) has obscured enough impact craters that crater-ages for even this youngest geologic unit are problematic. Nevertheless, the crater density of *Ch'al*, regions of greatest frequency (Calef et al., 2022) provides a lower bound on the age of the crater floor of 3.45 Ga (Goudge et al., 2015).

Because the floor of Jezero crater was anticipated to consist of sediments associated with the fluvial system that deposited the delta, the ability to distinguish between sediments and igneous rocks has been an important debate in the initial analysis of observations on the crater floor traverse. For this reason, we have dwelled on the

characteristics of exposures observed along the traverse that distinguish basaltic lavas from sedimentary deposits, particularly those characteristics that are manifested in eroded sections and exhumed surfaces. The identification of these has benefitted from advances in the terrestrial studies of lava flow internal structure since the 1980's that have identified many structures and patterns visible in the section that are diagnostic of various types of lava flow emplacements, particularly pahoehoe and aa. This includes sheet flows, breakout geometries, character of lava inflation in section, vesicle size distributions and zonation, jointing patterns (other than columnar joints), and styles and diagnostic features of surface erosion (Aubele et al., 1988; Cashman & Kauahikaua, 1997; Crumpler, 2001, 2002, 2009; Sahagian, 1985; Self et al., 1998; Walker, 1989, 1991; Wilmoth & Walker, 1993). Based on this background, outcrops of the *Ch'al member* and the *Rochette member* are identified as the first outcrop sections of lava flows visited by a rover on Mars and provide some insight into the varied styles of emplacement. Although these characteristics are not as yet widely appreciated in the planetary science community, they are likely to play an important role in understanding martian in situ geologic exposures, particularly as exploration proceeds into more complex and deeply exposed sections of the crust elsewhere.

The ability to distinguish between pits in rocks originating from erosion processes and primary vesicles in volcanic rocks has been a source of confusion and contention in planetary surface studies (e.g., Head et al., 2011). This debate has been equally problematic at the current site. The proposed origins of pits in rocks observed on the floor of Jezero crater and at lander and rover sites on Mars since Viking included vesicles, aeolian ventifact mechanisms, plucking of pebbles in conglomerates, and dissolution weathering. While it is acknowledged that distinguishing between these origins is difficult for any one example using remote observations on landers or rovers, as with many field studies, the context and local outcrop characteristics are considered here to be the principal means of distinguishing between the two origins, particularly where other characteristics support a given lithology of the host rock.

More detailed analysis based on the current understanding of lava sections permits speculation about the significance of differences in lava sections. For example, the *Rochette member* lavas display many of the characteristics of pahoehoe lava, including inflation structure, but the *Ch'al member* lava bear many of the characteristics of aa lava flows, including massive interiors showing little vesicle zonation and randomly oriented arcuate joints (non-orthogonal jointing). Both are observed in the section, a result not previously acquired in previous rover sites. The importance of this is that it confirms that many of the internal characteristics and structures used to identify lava flow emplacements appear to be viable for martian lava flows. This may prove useful for future missions where complex stratigraphic sections are observed and lava flows are observed only in the section.

The protoliths and origins of the principal polygonally jointed units ubiquitous in the *OEB Landing Site* and farther south along the traverse, the *Nataani member* and the *Roubion member*, remain enigmatic. Many examples of core-stone-like alteration, typical of deeply weathered crystalline rocks on Earth, and the findings from proximity measurements, including abrasions, are indicative of deep alteration of formerly massive geologic units bearing few internal structures or finer petrographic relationships indicative of their emplacement before alteration. There is suggestive evidence that the upper sections of these are more deeply altered than the lower parts. For example, the *Artuby member*, which overlies the *Roubion member*, is foliated and layered at scales from centimeters and millimeters and bears some core stone-like characteristics seen in section at the sol 175 location that are comparable to the dark protuberances on horizontal surfaces of the *Roubion member*, particularly in proximity to the *Rochette member* contact. This might imply that the *Artuby member* is simply an upper "facies" of *Roubion* that was closer to the surface and experienced more substantial weathering, a weathering that diminishes downward into the *Roubion member* protolith. Dark protuberances on *Nataani* in proximity to the contact with *Ch'al* exposures might represent something similar. While an *Artuby*-like unit atop *Nataani* was not observed in the section, the interface between the *Nataani member* and the *Ch'al* block "Sid" (Figure 6d) is similar to *Artuby*-type foliations and fine laminations suggestive of a potentially similar weathering sequence in the upper *Nataani member*. These could be examples of the deep weathering of *Nataani* and *Roubion* protoliths prior to the emplacement of *Ch'al* and *Rochette* lava, respectively. Assessment of mineral and elemental chemistry between *Roubion* and *Artuby*, particularly mineralogy and elemental abundances in the *Artuby member* consistent with aqueous alteration of something with *Roubion member* elemental and mineralogical characteristics, would be necessary to identify this if it occurs.

4.2. Stratigraphy

The tentative stratigraphic sequence from in situ mapping used here (Figures 19b and 20) is one of several adopted from differing observational methods. Further work remains to be done, including the resolution of ques-

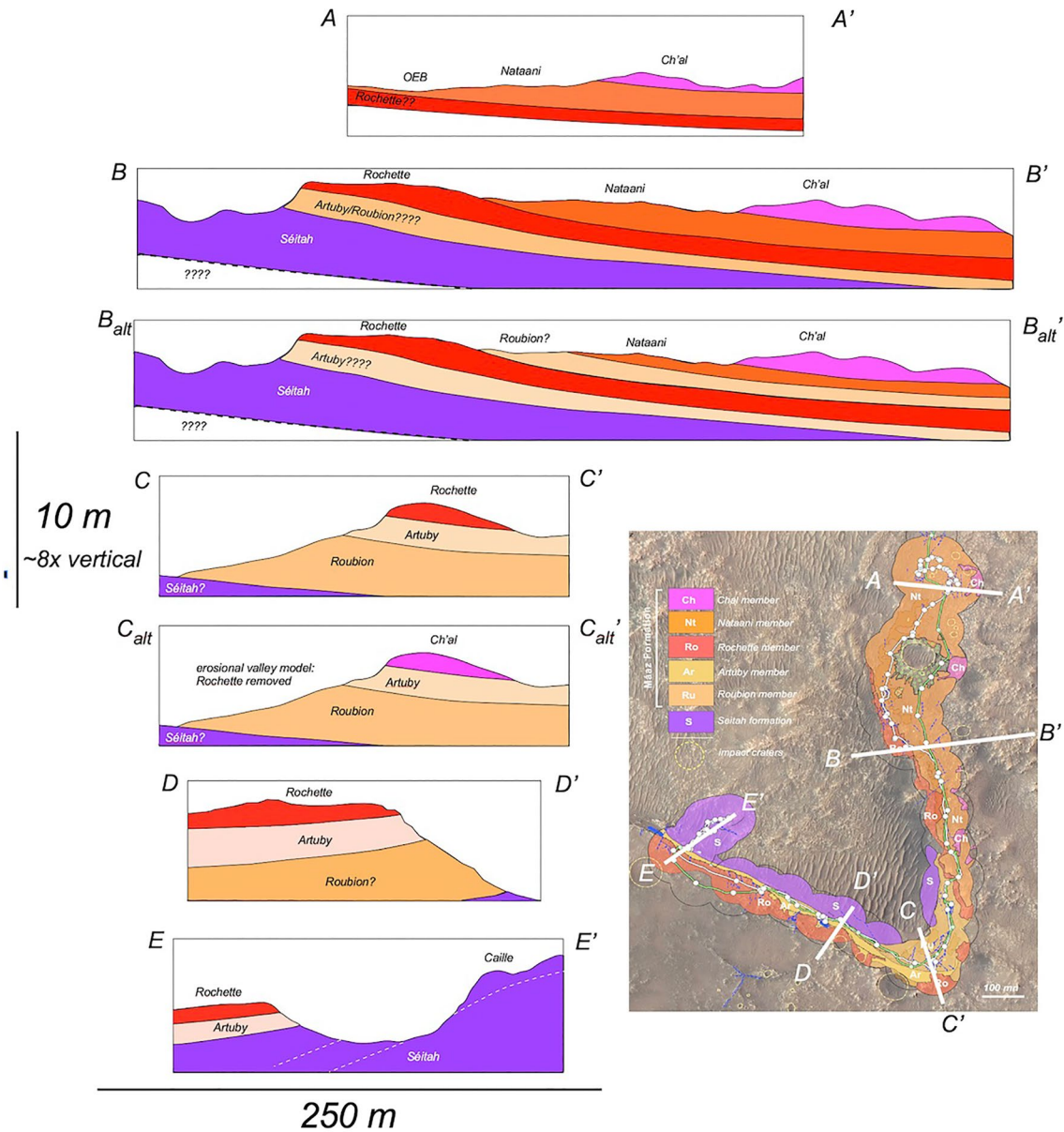


Figure 20. Speculative geologic sections based on geologic context mapping results at several locations along the traverse. Alternative stratigraphic sequences, discussed in the text (**B_{alt}** and **C_{alt}** in this graphic), are shown. In general, the stratigraphic sequence dips away from the contact between the *Séítah* and *Mázaz* formations.

tions about correlations between outcrops and determining reliable estimates of unit thicknesses. The differences in proposed stratigraphic sequences are representative of the difficulties in confirming some of these basic stratigraphic questions based on additional challenges that occur associated with correlation of the spectral, mineralogic, and elemental abundances from site to site. The following addresses some of the observations that challenge this working stratigraphy from the perspective of in situ observations.

The stratigraphic relations are clear in some locations but remain uncertain in others, as is often the case in field studies where observations are restricted to reconnaissance style mapping. The section sequence appears well-determined at the *OEB Landing Site* where *Ch'al* member outcrops rest on the *Nataani* member. However, the actual interface between *Ch'al* and *Nataani* members is not well exposed. We cannot determine whether the contact is an unconformity developed over substantial time with intervening erosion or whether it is a simple disconformity developed over an unknown time interval, or whether it is conformable.

The *Rochette member* at Mure overlies the *Artuby member*, and the *Artuby member* overlies what is locally identified as *Roubion member*. It is also unclear to what extent the contact is conformable and represents a continuous sequence or whether significant weathering occurred between the three units. The *Rochette-Artuby member* assemblage also overlies the exposures of the *Séítah formation*, confirming that *Mááz formation* overlies *Séítah formation*, again with an unknown time interval between the two. The contact between the *Mááz formation* and the *Séítah formation* along the escarpment separating the two does not lie at a uniform elevation. From the vicinity of the landing site to Mure at the southernmost end of the traverse, the elevation of the contact descends approximately 15 m. From Mure northwestward to the point of traverse into *Séítah*, the elevation of the contact ascends approximately 15 m. This means that the contact is not at a uniform elevation and either the apparent deformation of the contact implied by the dips away from *Séítah* has elevated the contact on the east and west margins that was at an originally uniform elevation or the lavas of the *Mááz formation* have simply flowed around the margins of *Séítah* along the general southeasterly sloping crater floor. The timing of the contact and the complete section relevant to any unconformity involving substantial differences in timing of emplacement may be better resolved with the return of samples (Simon, Hickman-Lewis, et al., 2023) in the future that have been carefully selected to assist in resolving these types of questions.

Places where the relationships are less clear include the relative positions of *Rochette* exposures and their correlation along the length of the escarpment, the vertical sequence of exposures visited in *Séítah* near the contact with *Artuby Ridge*, and the position and timing of the anomalous *Content member* atop the visited *Séítah* hill. The correlation of *Rochette* members with dense reflectors along the eastern escarpment remains a reasonable hypothesis rather than an observation, as does the identification of the basaltic rocks along the escarpment bounding *Séítah* on the east segment of the traverse as the same *Rochette* basalt capping *Artuby Ridge*. There remains the possibility that (a) the eastern escarpment “*Rochette*” is a later lava flow following relief at the *Séítah-Mááz* contact and correspondingly unknown stratigraphic relationship with *Ch'al*, and (b) the two separate occurrences of *Rochettes members* are different units of unknown stratigraphic relationship. The stratigraphy presented here assumes that the two “*Rochette*” occurrences are the same unit.

More problematic are questions arising from the mapped distribution of geologic units and transitions between otherwise well-understood sections. For example, the southward decline between sol 130 and 134 in the occurrence of *Nataani member* exposures (Figure 11) and the proximity of apparent *Ch'al* and *Rochette* exposures are not easily explained. The abrupt transition to the *Roubion member* capped by lavas between the sol 135–168 locations (Figure 13) is suspiciously similar to the *Nataani-Ch'al* sections to the north. Several hypotheses can be suggested that would resolve these questions (Figure 20) but create additional complexities. It is assumed from panoramic observations that the basaltic rocks exposed along the escarpment between the sol 130–134 locations are *Rochette* as was observed to the north. However, it is possible that *Ch'al* lava invaded the surface in this area during emplacement, moving from the east to fill in the terrain which descends abruptly. Either erosion prior to *Ch'al member* emplacement or, given the penchant for scissors-type fault along the escarpment, a fault in the section in this area might be responsible. A consequence of this scenario is that the *Roubion* exposures beginning on sol 135 and southward might be *Nataani member* and the basalts to the east of the valley here could be the *Ch'al member*. Mineral and spectral results on what are presumed to be *Rochette* basalts between sol 130–134 suggest that these units could be *Ch'al member*. Initial results on *Roubion* indicate that it is chemically and spectrally distinct from *Nataani* (Horgan, Rice, et al., 2022). Additional analysis will be necessary to test these hypotheses. To summarize, the section as mapped along this part (sol 135–168) of the traverse is interpreted to mean that *Roubion* is here overlain by capping dark rocks of the *Rochette member*, but some spectral observations suggest that it is instead. If this is the case, *Ch'al*. Horgan, Rice, et al. (2022) also make a good case that *Nataani member* lies between *Roubion* and *Ch'al*.

The *Content member* is anomalous because the absence of observed olivine implies that it is distinct from the surrounding *Séítah* rocks that are interpreted as rocks with intrusive cumulate textures. We have concluded that the *Content member* is probably part of the *Mááz formation* and that it was likely emplaced on a surface now isolated from its former continuation and connection with the *Rochette member* capping the *Artuby Ridge*. This would imply a significant unconformity across a former *Séítah* rock volume that is now deeply eroded, a hypothesis that cannot be tested with available stratigraphic information.

Potential Alternative stratigraphies. Due to the elusive nature of clear contact relations and lithologic identification along portions of the traverse, several alternatives to the stratigraphy presented here have been identified

(Horgan, Rice, et al., 2022; Simon, Amundsen, et al., 2022). Alternative stratigraphies can arise from differences in the assumed significance of textures and morphologies, spectral detection, RIMFAX interpretations and lithologic identification. Despite these differences in interpretation (e.g., Horgan, Rice, et al., 2022), similarities in the basic stratigraphy for the traverse as a whole are reflected in the results across studies.

More specifically, for the *Máaz formation*: (a) It is possible that the Rochette member is absent in the traverse section between sols 135 (“paver valley”) and sol 160 (Mure). As discussed above, this is potentially because it represents a laterally discontinuous lava sheet or because it is eroded here. In these locations, the apparent dark, angular rocks capping the *Roubion member* could be a local extension of *Ch'al member* lava; (b) the *Artuby member* may pinch out to the north and is only visible from Mure through the Artuby Ridge section. For *Séítah*: The section below the *Issole-Séítah undivided member* may be combined into just the *Bastide member*, that is, the *Brac and Caille members* may be simple sub-facies of a larger unit, the *Bastide member*. *These are all viable alternatives given the limited nature of the sections observed.*

4.3. Structure

At many locations, the contact between *Séítah* and *Máaz formations* sections dip away from the *Séítah* region with the relatively steep dips (5–20°), both within the margins of *Séítah* and overlying *Máaz formations*. Simple interpretive geologic sections at approximately right angles to the escarpment using the identified stratigraphic sequences can be constructed (Figure 20).

It is undetermined whether these dips are primary emplacements or represent the deformation of the sections. We cannot rule out the possibility that layers within the section are draped over some underlying regional relief. If the latter, then many of the long narrow troughs and fractures oriented both parallel to and at right angles to the margins of *Séítah* within the *Máaz formation* could result from the strain associated with the deformation. Alternatively, an initial relief imposed due to long-term uplift of *Séítah* limited on-lap by *Máaz formation* lavas was followed by continued uplift and subsequent fracturing and deformation of *Máaz formation* units. The origins of such uplift, if it occurred, remain unknown (Farley et al., 2022), but the chaotically eroded and broken terrain throughout *Séítah* would result from early fracturing and faulting in the brittle overburden that initiated the complex erosion within *Séítah*. If the uplift occurred gradually and continued over a sufficiently long period of time, an unconformable erosion surface could have also developed on which the early *Máaz formation* units were emplaced before becoming further deformed during the continued stages of uplift.

5. Conclusions

In situ mapping using terrestrial field geologic mapping method documents the distribution and principal stratigraphic relationships between 9 bedrock geologic units and a variety of regolith types on the Jezero Crater floor. While all field geologic maps represent a form of hypothesis, by organizing the distribution of outcrop exposures into a representative best-fit to observations, we think that the final maps provide a basis for better understanding the context of observations and may lead to better understanding of returned samples from this part of the Perseverance traverse.

The mapping process is relatively straightforward and its reliability is subject to variations in image geometries. However, until now the systematic methods of field mapping and recording the mapping confidence limits have been incompletely documented and the development of codified methods for recording in situ mapping as shown in this analysis represents a milestone in the field geologic mapping process on any planet. Application, additional development, and standardization of in situ mapping used here will be applicable to the detailed documentation of sites of future robotic and human traverses on Mars and other planetary surfaces. The advent of aerial platforms, as demonstrated by *Ingenuity* imaging and the examples shown here (e.g., Figure 11d), also promises to provide perspectives enabling mapping beyond the limits of traverse observations. These will be vital to future surface missions, where traverses and reconnaissance-style mapping will likely remain the norm for surface geological studies.

Preliminary efforts to match the radar sounding observations with surface in situ map results are encouraging. Effective understanding of radar sounding results is not a simple process, but early qualitative fitting, including the obvious utility in identifying dipping reflectors along the escarpment, demonstrate that future efforts to

merge surface in situ geologic mapping and radar sounding results promise to extend surface geologic detail meters into the substrate. Many examples of inferred subsurface unconformities and lateral discontinuities arising from buried faults and anomalous bodies, currently only hypotheses, could be tested more rigorously with radar sounding results.

Interpretation of the mapping is challenging on the crater floor due to the extensive erosion, significant bedrock alteration, structural complexities, and limited resources of time and traverses necessary for a more thorough understanding of the geologic context. Nonetheless, the mapping represents a source document recording the context of the proximity science, a starting point for a more detailed analysis of the samples collected for return to Earth, and the context of observations made during Perseverance's traverse.

Data Availability Statement

The data used in this research are available on the Planetary Data System (PDS) 20 August 2021, 22 November 2021 March 2022, and 22 July 2022 releases, <https://pds-geosciences.wustl.edu/missions/mars2020/index.htm>. The GIS files containing the shapefiles for the geologic mapping discussed in this manuscript are available at: Crumpler (2023), "In Situ Geologic Context Map: Mars 2020 Perseverance Rover Observations—shape files," <https://doi.org/10.5281/zenodo.7545299>.

References

- AIPG (1961). Code of stratigraphic nomenclature. *Bulletin of the American Institute of Petroleum Geologist*, 45, 645–665. <https://doi.org/10.1306/BC743685-16BE-11D7-8645000102C1865D>
- Allwood, A. C., Wade, L. A., Foote, M. C., Elam, W. T., Hurowitz, J. A., Battel, S., et al. (2020). PIXL: Planetary instrument for X-ray lithochemistry. *Space Science Reviews*, 216(8), 1–132.
- Alwmark, S., Horgan, B., Udry, A., Bechtold, A., Fagents, S., Ravanis, E., et al. (2023). Diverse lava flow morphologies in the stratigraphy of the Jezero crater floor. *Journal of Geophysical Research: Planets*, 128, e2022JE007446. <https://doi.org/10.1029/2022JE007446>
- Aubele, J. C., Crumpler, L. S., & Elston, W. E. (1988). Vesicle zonation and vertical structure of basalt flows. *Journal of Volcanology and Geothermal Research*, 35(4), 349–374. [https://doi.org/10.1016/0377-0273\(88\)90028-5](https://doi.org/10.1016/0377-0273(88)90028-5)
- Balaram, J. (2021). Mars 2020 helicopter camera suite bundle. *NASA Planetary Data System*. <https://doi.org/10.17189/1522845>
- Barnes, J. W. (1991). *Basic geological mapping* (2nd ed.). Halstead Press/Wiley.
- Beaty, D. W., Grady, M. M., McSween, H. Y., Sefton-Nash, E., Carrier, B. L., Altieri, F., et al. (2019). The potential science and engineering value of samples delivered to Earth by Mars sample return. *Meteoritics & Planetary Sciences*, 54, S3–S152. <https://doi.org/10.1111/maps.13242>
- Beegle, L. (2021). *Mars 2020 SHERLOC bundle*. *NASA Planetary Data System*. <https://doi.org/10.17189/1522643>
- Bell, J. F., & Maki, J. M. (2021). Mars 2020 mast camera zoom bundle. *NASA Planetary Data System*. <https://doi.org/10.17189/1522843>
- Bell, J. F., Maki, J. N., Mehall, G. L., Ravine, M. A., Caplinger, M. A., Bailey, Z. J., et al. (2022). The Mars 2020 perseverance rover mast camera zoom (Mastcam-Z) multispectral, stereoscopic imaging investigation. *Space Science Reviews*, 217(1), 1–40. <https://doi.org/10.1007/s11214-020-00755-x>
- Bhartia, R., Beegle, L. W., DeFlores, L., Abbey, W., Hollis, J., Uckert, K., et al. (2021). Perseverance's Scanning Habitable Environments with Raman and Luminescence for Organics and Chemicals (SHERLOC) Investigation. *Space Science Reviews*, 17, 58. <https://doi.org/10.1007/s11214-021-00812-z>
- Brown, A. J., Viviano, C. E., & Goudge, T. A. (2020). Olivine-carbonate mineralogy of the Jezero Crater region. *Journal of Geophysical Research: Planets*, 125(3). <https://doi.org/10.1029/2019JE006011>
- Calef, F. J., III, Alwmark, S., Herd, C. D. K., Simon, J. I., & Shuster, D. (2022). Crater retention observations of the crater floor–fractured rough unit in Jezero Crater. In *53rd Lunar and Planetary Science Conference*. abstract 1805.
- Cashman, K. V., & Kauahikaua, J. P. (1997). Reevaluation of vesicle distributions in basaltic lava flows. *Geology*, 25(5), 419–422. [https://doi.org/10.1130/0091-7613\(1997\)025<0419:ROVDIB>2.3.CO;2](https://doi.org/10.1130/0091-7613(1997)025<0419:ROVDIB>2.3.CO;2)
- Cohee, G. V. (1974). *Stratigraphic nomenclature in reports of the U.S. Geological Survey reports* (p. 45). United States Geological Survey Publications, U.S. Government Printing Office. <https://doi.org/10.3133/70047747>
- Compton, R. R. (1985). *Geology in the field*. Wiley.
- Crumpler, L. S. (2001). *Vesicles in surface rocks: Detection, analysis and significance: Lunar and Planetary Science Conference 32, abstracts*. LPI.
- Crumpler, L. S. (2002). Vesicularity and fracture spacing of rocks on degraded lava flows: Applicability to estimates of atmospheric density on early Mars. *Lunar and Planetary Science Conference*, 33. abstract no.1896.
- Crumpler, L. S., (2009). *Lava flow vesicularity on Earth and Mars controlled by equilibrium De-gassing*. Geological Society of America Abstracts with Programs, Vol. 41, No. 7, Paper No. 95-3, (p. 259).
- Crumpler, L. S., Arvidson, R. E., Bell, J., Clark, B. C., Cohen, B. A., Gellert, R., et al. (2015). Context of ancient aqueous environments on Mars from in situ geologic mapping at endeavour crater. *Journal of Geophysical Research*, 120(3), 538–569. <https://doi.org/10.1002/2014JE004699>
- Crumpler, L. S., Arvidson, R. E., Mittlefehldt, D. W., Grant, J. A., & Farrand, W. H. (2020). Results from the first geologic traverse on the topographic rim of a complex impact crater, Endeavour Crater, Mars. *Geology*, 48(3), 252–257. <https://doi.org/10.1130/G46903.1>
- Crumpler, L. S., Arvidson, R. E., Squyres, S. W., McCoy, T., Yingst, A., Ruff, S., et al. (2011). Field reconnaissance geologic mapping of the Columbia hills, Mars, based on Mars exploration rover spirit and MRO HiRISE observations. *Journal of Geophysical Research*, 116, E00F24. <https://doi.org/10.1029/2010JE003749>
- Crumpler, L. S., Horgan, B., Simon, J., Stack, K., Alwmark, S., Dromart, G., et al. (2023). GIS shapefiles for in situ geologic map based on Mars 2020 perseverance rover observations [Dataset]. *Journal of Geophysical Research-Planets* (Version 1). Zenodo. <https://doi.org/10.5281/zenodo.7545299>

Acknowledgments

This paper benefited significantly from thorough reviews and suggestions by David Crown and an anonymous reviewer. Funding for LSC and most of the co-authors was provided by NASA through the Mars 2020 Program, Mars Exploration Program, or Participating Scientist Program (LSC, Grant 80NSSC21K0327). CDKH is supported by Canadian Space Agency Grant 20EXPMARS.

- Farley, K. A., Stack, K. M., Horgan, B. H. N., Tarnas, J., Sun, V. Z., Shuster, D. L., et al. (2022). Aqueously altered igneous rocks on the floor of Jezero crater, Mars. *Science Advances*, 377(6614). <https://doi.org/10.1126/science.abo2196>
- Ferguson, R. L., Hare, T. M., Mayer, D. P., Galuszka, D. M., Redding, B. L., Smith, E. D., et al. (2020). Mars 2020 Terrain relative navigation flight product generation: Digital terrain model and orthorectified image mosaics. *Lunar and Planetary Science Conference*, 51, abstract.
- Goudge, T. A., Mustard, J. F., Head, J. W., Fassett, C. I., & Wiseman, S. M. (2015). Assessing the mineralogy of the watershed and fan deposits of the Jezero crater paleolake system, Mars. *Journal of Geophysical Research: Planets*, 120(4), 775–808. <https://doi.org/10.1002/2014JE004782>
- Hamran, S.-E., Paige, D. A., Allwood, A., Amundsen, H. E. F., Berger, T., Brovoll, S., et al. (2022). Ground penetrating radar observations of subsurface structures in the floor of Jezero crater, Mars. *Science Advances*, 8(34), eabp8564. <https://doi.org/10.1126/sciadv.abp8564>
- Hamran, S.-E., Paige, D. A., Amundsen, H. E. F., Berger, T., Brovoll, S., Carter, L., et al. (2020). Radar imager for Mars' subsurface experiment—RIMFAX. *Space Science Reviews*, 216(8), 128. <https://doi.org/10.1007/s11214-020-00740-4>
- Head, J. W., Kreslavsky, M. A., & Marchant, D. R. (2011). Pitted rock surfaces on Mars: A mechanism of formation by transient melting of snow and ice. *Journal of Geophysical Research*, 116(E9), E09007. <https://doi.org/10.1029/2011JE003826>
- Herkenhoff, K. E., Sullivan, R. J., Newman, C. E., Paar, G., Baker, G., Baker, M., Viúdez-Moreiras, D., et al. (2023). Comparison of ventifact orientations and recent wind direction indicators on the floor of Jezero Crater, Mars. *Journal of Geophysical Research: Planets*, 128, e2022JE007599. <https://doi.org/10.1029/2022JE007599>
- Horgan, B., Rice, M., Garczynski, B., Johnson, J., Stack-Morgan, K., Vaughan, A., et al. (2023). Mineralogy, morphology, and geochronological significance of the Máaz formation and the Jezero Crater floor. In *53rd Lunar and Planetary Science Conference*. abstract 1680.
- Horgan, B. H., Anderson, R. B., Dromart, G., Amador, E. S., & Rice, M. S. (2020). The mineral diversity of Jezero crater: Evidence for possible lacustrine carbonates on Mars. *Icarus*, 339, 113526. <https://doi.org/10.1016/j.icarus.2019.113526>
- Horgan, B., Udry, A., Rice, M., Alwmark, S., Amundsen, H. E. F., Bell, J. F. III, et al. (2023). Mineralogy, morphology, and emplacement history of the Maaz formation on the Jezero crater floor from orbital and rover observations. *Journal of Geophysical Research: Planets*, 128, e2022JE007612. <https://doi.org/10.1029/2022JE007612>
- Jerram, D. A., Cheadle, M. J., & Philippot, A. R. (2003). Quantifying the building blocks of igneous rocks: Are clustered crystal frameworks the foundation? *Journal of Petrology*, 44(11), 2033–2052. <https://doi.org/10.1093/petrology/egg069>
- Liu, Y., Tice, M. M., Schmidt, M. E., Treiman, A. H., Kizovski, T. V., Hurowitz, J. A., et al. (2022). An olivine cumulate outcrop on the floor of Jezero crater, Mars. *Science*, 377(6614), 1513–1519. <https://doi.org/10.1126/science.abo2756>
- Macdonald, G. A. (1953). Pahoehoe, aa, and block lava. *American Journal of Science*, 251(3), 169–191. <https://doi.org/10.2475/ajs.251.3.169>
- Maki, J. (2020). Mars 2020 navigation cameras bundle, mosaic products. *NASA Planetary Data System*. <https://doi.org/10.17189/OSXN-ZB41>
- Maki, J., Gruel, N. D., McKinney, C., Ravine, M. A., Morales, M., Lee, D., et al. (2021). The Mars 2020 engineering cameras and microphone on the perseverance rover: A next-generation imaging system for Mars exploration (2021). *Space Science Reviews*, 216(8), 137. <https://doi.org/10.1007/s11214-020-00765-9>
- Maurice, S., & Wiens, R. C. (2021). *Mars 2020 SuperCam bundle*. NASA Planetary Data System. <https://doi.org/10.17189/1522646>
- Maurice, S., Wiens, R. C., Bernardi, P., Caïs, P., Robinson, S., Nelson, T., et al. (2021). The SuperCam instrument suite on the Mars 2020 rover: Science objectives and Mast-Unit description. *Space Science Reviews*, 217(3), 1–108.
- MEPAG E2E-iSAG. (2011). Planning for Mars returned sample science: Final report of the MSR end-to-end international science analysis group (E2E-iSAG). *Astrobiology*, 12, 175–230.
- Sahagian, D. L. (1985). Bubble migration and coalescence during the solidification of basaltic lava flows. *The Journal of Geology*, 93(2), 205–211. <https://doi.org/10.1086/628942>
- Schmidt, M. E., Allwood, A., Christian, J., Clark, B. C., Flannery, D., Hennecke, J., et al. (2022). Highly differentiated basaltic lavas examined by PIXL in Jezero Crater. In *53rd Lunar and Planetary Science Conference*. abstract 1530.
- Self, S., Keszthelyi, L., & Thordarson, T. (1998). The importance of pahoehoe. *Annual Review of Earth and Planetary Sciences*, 26(1), 81–110. <https://doi.org/10.1146/annurev.earth.26.1.81>
- Simon, J., Amundsen, H. E. F., Beegle, L. W., Bell, J., Benison, K. C., Berger, E. L., et al. (2023). Sampling of Jezero crater Máaz formation by Mars 2020 Perseverance rover. In *53th Lunar and Planetary Science Conference*. abstract 1294.
- Simon, J., Benison, K. C., Bosak, T., Brown, A. J., Calef, F., Cohen, B. A., et al. (2021). *Mars 2020's first sample: The fractured rough rock unit on the floor of Jezero Crater*. AGU meeting abstract. P21B-02.
- Simon, J. I., Hickman-Lewis, K., Cohen, B. A., Mayhew, L. E., Shuster, D. L., Debaille, V., et al. (2023). Samples collected from the floor of Jezero Crater with the Mars 2020 Perseverance rover. *Journal of Geophysical Research: Planets*, 128, e2022JE007474. <https://doi.org/10.1029/2022JE007474>
- Stack, K. M., Williams, N. R., Calef, F., Sun, V. Z., Williford, K. H., Farley, K. A., et al. (2020). Field site in Jezero Crater constructed by the Mars 2020 science team. *Space Science Reviews*, 216(8), 127. <https://doi.org/10.1007/s11214-020-00739-x>
- Sullivan, R., Baker, M., Golombek, M., Herkenhoff, K., Newman, C., & Tate, C. (2022). Enigmatic large bedforms on the floor of Jezero Crater. In *53rd Lunar and Planetary Science Conference*. abstract 2887.
- Sullivan, R., Banfield, D., Bell, J. F., Calvin, W., Fike, D., Golombek, M., et al. (2005). Aeolian processes at the Mars exploration rover meridiani planum landing site. *Nature*, 436(7047), 58–61. <https://doi.org/10.1038/nature03641>
- Sun, V. Z., Hand, K. P., Stack, K. M., Farley, K. A., Milkovich, S., Kronyak, R., et al. (2022). Exploring the Jezero Crater floor: Overview of results from the Mars 2020 Perseverance rover's first science campaign. In *53rd Lunar and Planetary Science Conference*. abstract 1798.
- Sun, V. Z., & Stack, K. M. (2020). Geologic map of Jezero crater and the Nili planum region, Mars. *Scientific investigations map*. U.S. Geological Survey. USGS Numbered Series 3464. <https://doi.org/10.3133/sim3464>
- Tate, C. D., Hayes, A. G., Crumpler, L. S., Gupta, S., & Nunez, J. I. (2022). Stratigraphic photogrammetric modeling of Séítah toe-dip area for stratigraphic analysis of Jezero Crater, Mars. In *53rd Lunar and Planetary Science Conference*. abstract 2956.
- Udry, A., Ostwald, A., Sautter, V., Cousin, A., Beyssac, O., Forni, O., et al. (2023). A Mars 2020 Perseverance SuperCam perspective on the igneous nature of the Máaz formation at Jezero crater and link with Séítah, Mars. *Journal of Geophysical Research: Planets*, 128, e2022JE007440. <https://doi.org/10.1029/2022JE007440>
- U.S. Geological Survey. (1958). Suggestions to authors of the reports of the United States geological Survey (5th ed., p. 255). Retrieved from <https://pubs.er.usgs.gov/publication/70058737>
- Vaughan, A., Minitti, M. E., Cardarelli, E. L., Johnson, J. R., Kah, L. C., Pilleri, P., et al. (2023). Regolith of the crater floor units, Jezero crater, Mars: Textures, composition, and implications for provenance. *Journal of Geophysical Research: Planets*, 128, e2022JE007437. <https://doi.org/10.1029/2022JE007437>
- Walker, G. P. L. (1989). Spongy pahoehoe in Hawaii: A study of vesicle-distribution patterns in basalt and their significance. *Bulletin of Volcanology*, 51(3), 199–209. <https://doi.org/10.1007/bf01067956>

- Walker, G. P. L. (1991). Structure, and origin by injection under surface crust, of tumuli, "lava rises," "lava-rise pits," and "lava inflation clefts" in Hawaii. *Bulletin of Volcanology*, 53(7), 546–558. <https://doi.org/10.1007/bf00298155>
- Wiens, R. C., Maurice, S., Robinson, S. H., Nelson, A. E., Cais, P., Bernardi, P., et al. (2020). The SuperCam instrument suite on the NASA Mars 2020 rover: Body unit and combined system tests. *Space Science Reviews*, 217, 4.
- Wiens, R. C., Udry, A., Beyssac, O., Quantin-Nataf, C., Mangold, N., Cousin, A. S., et al. (2022). Compositionally and density stratified igneous terrain in Jezero crater, Mars. *Science Advances*, 8(34). <https://doi.org/10.1126/sciadv.abo3399>
- Wilmoth, R. A., & Walker, G. P. L. (1993). P-Type and S-type pahoehoe: A study of vesicle distribution patterns in Hawaiian lava flows. *Journal of Volcanology and Geothermal Research*, 55(1–2), 129–142. [https://doi.org/10.1016/0377-0273\(93\)90094-8](https://doi.org/10.1016/0377-0273(93)90094-8)

Erratum

In the originally published version of this article, co-author Gilles Dromart's name was inadvertently transposed as D. Gilles in the author list, article citation, and author contributions section. The author's name has now been corrected to G. Dromart in these sections, and this version may be considered the authoritative version of record.